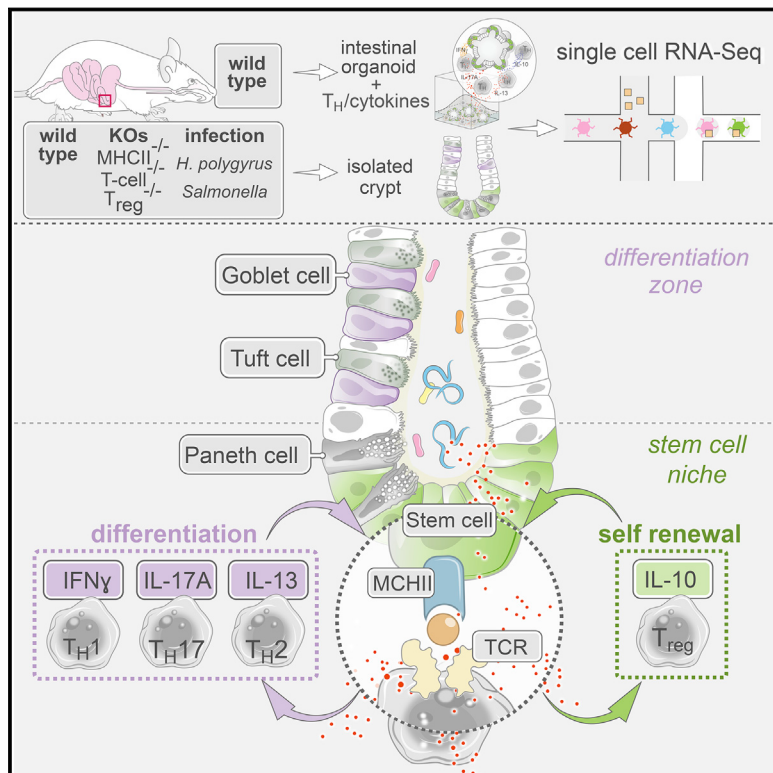


T Helper Cell Cytokines Modulate Intestinal Stem Cell Renewal and Differentiation

Graphical Abstract



Authors

Moshe Biton, Adam L. Haber,
Noga Rogel, ..., Omer H. Yilmaz,
Aviv Regev, Ramnik J. Xavier

Correspondence

aregev@broadinstitute.org (A.R.),
xavier@molbio.mgh.harvard.edu (R.J.X.)

In Brief

Intestinal stem cells act as non-conventional antigen presenting cells, and these interactions with T helper cells modulate ISC renewal and differentiation to shape the intestine.

Highlights

- Intestinal stem cells (ISCs) are non-conventional antigen-presenting cells by MHCII
- Interactions between ISCs and T helper subsets modulate distinct ISC fates
- Epithelial MHCII is important for epithelial-cell remodeling following infection
- Regulatory T cells and their key cytokine IL-10 support ISC renewal

T Helper Cell Cytokines Modulate Intestinal Stem Cell Renewal and Differentiation

Moshe Biton,^{1,2,19} Adam L. Haber,^{1,19} Noga Rogel,^{1,19} Grace Burgin,¹ Semir Beyaz,^{3,4,5} Alexandra Schnell,⁶ Orr Ashenberg,¹ Chien-Wen Su,⁷ Christopher Smillie,¹ Karthik Shekhar,¹ Zuoja Chen,⁶ Chuan Wu,⁶ Jose Ordovas-Montanes,^{8,9,10,11} David Alvarez,¹² Rebecca H. Herbst,^{1,13} Mei Zhang,⁷ Itay Tirosh,^{1,14} Danielle Dionne,¹ Lan T. Nguyen,¹ Michael E. Xifaras,³ Alex K. Shalek,^{8,9,10,11} Ulrich H. von Andrian,¹² Daniel B. Graham,⁹ Orit Rozenblatt-Rosen,¹ Hai Ning Shi,⁷ Vijay Kuchroo,^{6,9} Omer H. Yilmaz,^{3,9,15} Aviv Regev,^{1,3,16,20,*} and Ramnik J. Xavier^{2,9,17,18,19,21,*}

¹Klarman Cell Observatory, Broad Institute of Harvard and MIT, Cambridge, MA 02142, USA

²Department of Molecular Biology, Massachusetts General Hospital, Boston, MA 02114, USA

³The David H. Koch Institute for Integrative Cancer Research at MIT, Department of Biology, MIT, Cambridge, MA 02139, USA

⁴Division of Hematology/Oncology, Boston Children's Hospital and Department of Pediatric Oncology, Dana-Farber Cancer Institute, Howard Hughes Medical Institute, Harvard Stem Cell Institute, Harvard Medical School, Boston, MA 02115, USA

⁵Cold Spring Harbor Laboratory, Cold Spring Harbor, NY 11724, USA

⁶Evergrande Center for Immunologic Diseases, Brigham and Women's Hospital, Harvard Medical School, Boston, MA, USA

⁷Mucosal Immunology and Biology Research Center, Massachusetts General Hospital and Harvard Medical School, Charlestown, MA 02129, USA

⁸Institute for Medical Engineering & Science (IMES) and Department of Chemistry, Massachusetts Institute of Technology (MIT), Cambridge, MA 02139, USA

⁹Broad Institute of Harvard and MIT, Cambridge, MA 02142, USA

¹⁰Ragon Institute of MGH, MIT, and Harvard, Cambridge, MA 02139, USA

¹¹The David H. Koch Institute for Integrative Cancer Research at MIT, Cambridge, MA 02142, USA

¹²Department of Microbiology & Immunobiology and Center for Immune Imaging, Harvard Medical School, Boston, MA 02115, USA

¹³Department of Systems Biology, Harvard Medical School, Boston, MA 02114, USA

¹⁴Department of Molecular Cell Biology, Weizmann Institute of Science, Rehovot 7610001, Israel

¹⁵Department of Pathology, Massachusetts General Hospital, Boston, MA 02114, USA

¹⁶Howard Hughes Medical Institute, Department of Biology, Massachusetts Institute of Technology, Cambridge, MA 02140, USA

¹⁷Gastrointestinal Unit and Center for the Study of Inflammatory Bowel Disease, Massachusetts General Hospital, Boston, MA 02114, USA

¹⁸Center for Microbiome Informatics and Therapeutics, MIT, Cambridge, MA 02139, USA

¹⁹These authors contributed equally

²⁰Senior author

²¹Lead Contact

*Correspondence: aregev@broadinstitute.org (A.R.), xavier@molbio.mgh.harvard.edu (R.J.X.)

<https://doi.org/10.1016/j.cell.2018.10.008>

SUMMARY

In the small intestine, a niche of accessory cell types supports the generation of mature epithelial cell types from intestinal stem cells (ISCs). It is unclear, however, if and how immune cells in the niche affect ISC fate or the balance between self-renewal and differentiation. Here, we use single-cell RNA sequencing (scRNA-seq) to identify MHC class II (MHCII) machinery enrichment in two subsets of Lgr5⁺ ISCs. We show that MHCII⁺ Lgr5⁺ ISCs are non-conventional antigen-presenting cells in co-cultures with CD4⁺ T helper (Th) cells. Stimulation of intestinal organoids with key Th cytokines affects Lgr5⁺ ISC renewal and differentiation in opposing ways: pro-inflammatory signals promote differentiation, while regulatory cells and cytokines reduce it. *In vivo* genetic perturbation of Th cells or MHCII expression on Lgr5⁺ ISCs impacts epithelial cell differentiation and IEC fate during infection. These interactions between Th cells and

Lgr5⁺ ISCs, thus, orchestrate tissue-wide responses to external signals.

INTRODUCTION

To maintain tissue homeostasis, the gut epithelium constantly regenerates by rapid proliferation and differentiation ([van der Flier and Clevers, 2009](#)), from intestinal stem cells (ISCs), to committed progenitors, to specific intestinal epithelial cell (IEC) types ([Barker et al., 2007; van der Flier and Clevers, 2009](#)). ISC differentiation depends on external signals from both epithelial and non-epithelial cells, especially stromal cells ([Degirmenci et al., 2018; Shoshkes-Carmel et al., 2018](#)).

Several studies have shown important roles for immune cells in tissue homeostasis. Tissue-resident innate immune cells can play a role in regeneration of the gut ([Lindemans et al., 2015; Saha et al., 2016](#)) and other tissues ([Aurora and Olson, 2014; Stappenbeck and Miyoshi, 2009](#)). Among adaptive immune cells, recent studies have implicated T regulatory cells (T_{regs}) in tissue regeneration processes in the muscles and lungs ([Arpaia et al., 2015; Burzyn et al., 2013](#)), and T cytotoxic cells were

shown to eliminate Lgr5⁺ ISCs via MHC class I (Agudo et al., 2018). Skin-resident T_{regs} were recently shown to help maintain hair follicle stem cell (HFSC) renewal via Notch signaling (Ali et al., 2017), but a similar role in the gut has not been reported.

Here, using single-cell RNA sequencing (scRNA-seq), we found Lgr5⁺ ISC subsets with enriched expression of MHC class II (MHCII) molecules. We showed that Lgr5⁺ ISCs stimulated with antigen can present to and interact with Th cells. We characterized the functional impact of ISC-T cell interactions in organoid assays and in mouse models during homeostasis or infections, finding opposing effects of key inflammatory and regulatory Th cells and cytokines on Lgr5⁺ ISC renewal and differentiation and highlighting a new functional axis for gut homeostasis.

RESULTS

High Expression of MHCII Genes by ISC Subsets

To search for an ISC-immune cell interaction, we queried our recent scRNA-seq data of 1,522 EpCAM⁺ intestinal epithelial cells (IECs) (Haber et al., 2017) from wild-type (WT) and Lgr5-GFP mice (Barker et al., 2007) for genes expressed by ISCs that encode cell surface or secreted proteins known to interact with immune cells. ISCs partitioned into three sets (ISC-I, -II, and -III) (Figures 1A and 1B), all expressing known stem cell markers, including Lgr5 (Figures 1D, S1A, and S1B; Table S1), consistent with recent reports (Yan et al., 2017). By expression signatures, flow cytometry, and immunofluorescence assays (IFA), we identified an ISC subset that is low-cycling (ISC-I), and two more proliferative ISC subsets (ISC-II and -III) (Figures S1C–S1E). All subsets are present in similar proportions in the duodenum, jejunum, and ileum (Figure S1F; STAR Methods). Pseudotime analysis (Haghverdi et al., 2015) suggested that ISC-I have the most stem-like features, while ISC-II and ISC-III are progressively more differentiated (Figures 1C, S1H, and S1I), although these may not reflect a developmental order as IECs can de-differentiate (Buczacki et al., 2013; Tetteh et al., 2016).

Querying annotated receptor genes (Ramilowski et al., 2015) that are differentially expressed (DE) between ISCs and the other IECs (Figure S1G; Table S2) identified Cd74, which encodes the invariant chain of the MHCII complex, as enriched in ISCs (Figures 1E, 1F, S1G, and S2A). This expression was enriched in ISC-II and ISC-III, which also co-expressed many other canonical components of the MHCII machinery and the non-canonical co-stimulatory molecules *Sectm1a* and *Sectm1b* (Howie et al., 2013; Wang et al., 2012) (Figure 1F). MHCII expression has been previously described in IECs (Bland and Warren, 1986; Thelemann et al., 2014), but its ISC enrichment was not reported. We validated enriched MHCII protein expression by Lgr5⁺ ISCs by fluorescence-activated cell sorting (FACS) and *in situ* in WT mice, and its absence in a constitutive MHCII knockout (KO) (Madsen et al., 1999) (Figures 1G, S2B, and S2C). We further showed that MHCII⁺ Lgr5⁺ ISCs (ISC-II and -III) are more proliferative than ISC-I (Figures S2D and S2E).

MHCII⁺ Lgr5⁺ ISCs Functionally Present Antigen to Th Cells

IECs have been previously shown to present class II antigens and interact with Th cells (Bland and Warren, 1986; Kaiserlian

et al., 1989). We hypothesized that among IECs, it is Lgr5⁺ ISCs that interact with Th cells via MHCII. Intravital imaging showed that Th cells are in close proximity to Lgr5⁺ ISCs in small intestinal crypts (Figure S3B, red arrows; Video S1).

To test this hypothesis, we sorted EpCAM⁺ cells, which contain Lgr5⁺ ISCs (Figure S1B), and cultured them with DQ-ovalbumin (DQ-Ova), a self-quenching conjugate of ovalbumin that fluoresces upon proteolytic degradation. (We could not use Lgr5-GFP⁺ cells, as the fluorescence of GFP and quenched DQ-Ova may overlap.) Approximately 10% of EpCAM⁺ cells had high fluorescence, compared to ~40% of dendritic cells (DCs) (Figure 2A). A stem cell signature was highly enriched in DQ-Ova⁺ EpCAM⁺ cells compared to all EpCAM⁺ cells by scRNA-seq (Figure 2B). Thus, ISCs within EpCAM⁺ cells largely account for their ability to process extracellular antigens.

Next, we showed that Lgr5⁺ ISCs activate Th cells *in vitro* in an antigen-specific manner. We enriched for EpCAM⁺-Lgr5-GFP^{high} ISCs, EpCAM⁺GFP[−] IECs (that include non-GFP Lgr5⁺ ISCs due to the mosaic nature of this mouse model), or DCs from the lamina propria (LP) of Lgr5-GFP mice (n = 9 mice). We co-cultured each subset in the presence of ovalbumin (Ova) peptide with naive OTII Th cells that specifically recognize Ova peptide 323–339-MHCII complexes (OTII) (STAR Methods). OTII cells co-cultured with EpCAM⁺GFP[−] cells led to a modest increase in interleukin 2 (IL-2) protein secretion as previously reported (Bland and Warren, 1986; Kaiserlian et al., 1989) (Figure 2C). Compared to EpCAM⁺GFP[−] cells, co-culture with Lgr5-GFP⁺ ISCs or DCs caused substantially higher OTII activation by IL-2 secretion (~3- and 21-fold higher, Figure 2C) and T cell proliferation (65.8% and 89.5% versus 32.6%, Figure S3A). These results indicate that *in vitro* Lgr5⁺ ISCs interact and activate naive Th cells via MHCII presentation of peptides.

Th Cytokines Regulate Lgr5⁺ ISC Renewal and Differentiation

To investigate the impact of the Th-ISCs interaction on ISCs, we next used an intestinal organoid culture in which immune cells are absent but can be added in a controlled manner (Figure S3D). We isolated the effect of MHCII by using prolonged cultured organoids (2 weeks) (Sato et al., 2009), in which Lgr5⁺ ISCs lose expression of MHCII (Figure S3C). We added to the organoid cultures either polarized, cytokine-producing, Th cell subsets (Th1, Th2, Th17, or inducible T_{reg} [iT_{reg}] cells) (Jäger et al., 2009) or their respective key cytokines (interferon gamma [$\text{IFN}\gamma$], IL-13, IL-17A, or IL-10). We also tested IL-22, as it shares the same receptor subunit with IL-10. IECs, including ISCs, expressed receptors for Th cytokines $\text{IFN}\gamma$, IL-13, IL-4, IL-17A, IL-10 (IL-10rb), and IL-22 (Figure S1J), although IL-10ra expression was detectable only in bulk quantitative PCR at low levels (data not shown), as previously reported (Denning et al., 2000). We collected scRNA-seq profiles for each condition. For the Th co-cultures, we computationally distinguished (post hoc) epithelial cells from T cells by their profiles. We confirmed by FACS that each Th subset expressed key cytokines and TFs prior to co-culture (data not shown), and we confirmed by scRNA-seq that they maintain this expression during co-culture (Figure S3E). However, *ex vivo* polarized Th cells did not fully recapitulate their *in vivo* counterparts: Th2

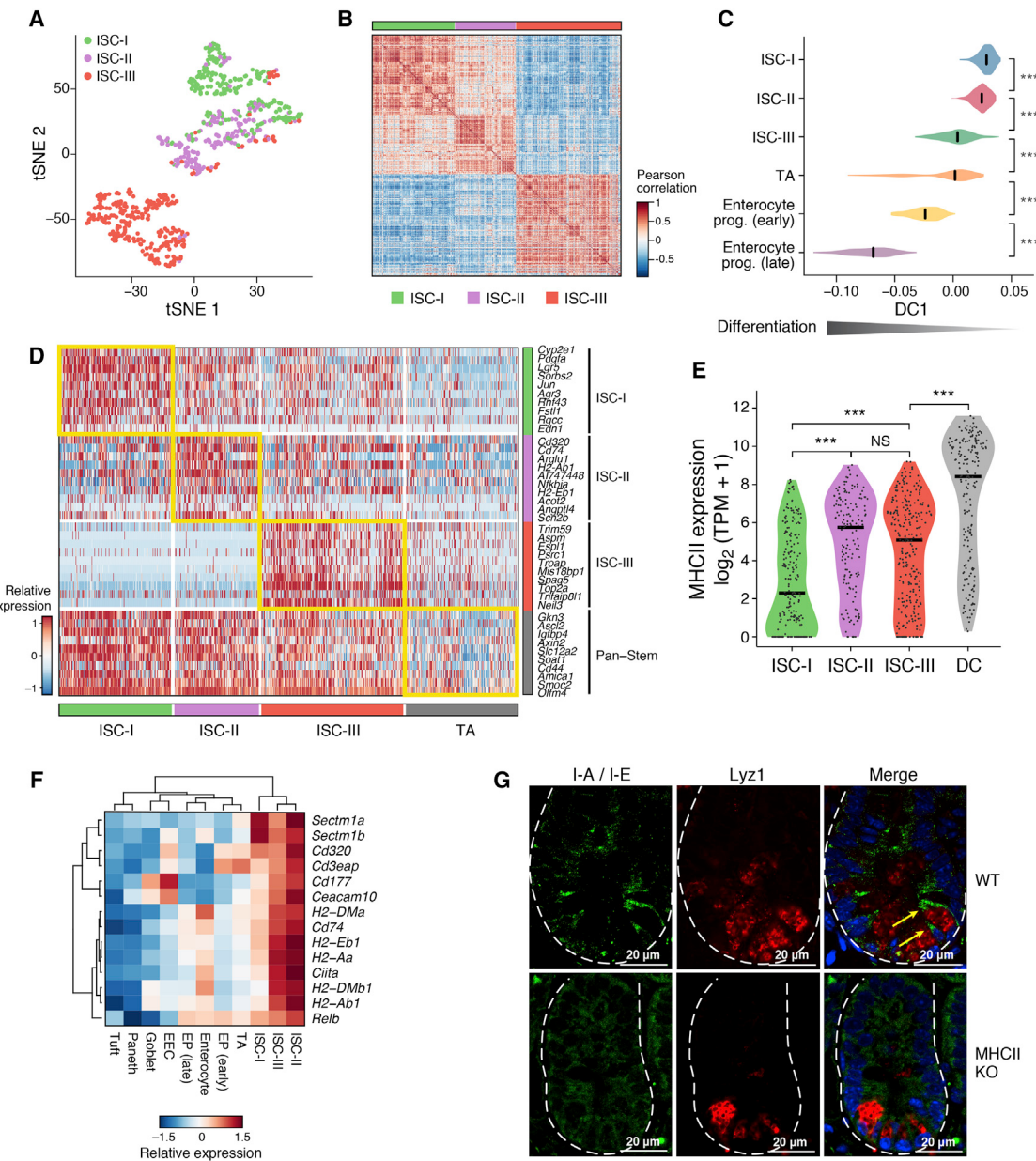


Figure 1. ScRNA-Seq Reveals MHCII Expression in Subsets of *Lgr5*⁺ ISCs

(A and B) Three subsets of *Lgr5*⁺ ISCs. A t-distributed stochastic neighbor embedding (tSNE) (A) and correlation matrix (B) of 637 ISCs identified by clustering of 1,522 cells by scRNA-seq. Color code: kNN-graph clusters and post hoc annotation. Heatmap (B) shows the Pearson correlation coefficient (r , color bar) between cell scores along the first 10 principal components.

(C) Differentiation pseudotime of ISC subsets. Distribution of DC-1 scores ("differentiation," x axis) for each cell cluster (y axis). Black bar: mean. *** $p < 0.0001$, Mann-Whitney U test.

(D) Gene signatures of ISC subsets. Relative expression level (row-wise Z score of $\log_2(\text{TPM} + 1)$ values, color bar) in 637 ISCs and 201 TA (columns, color code as in (A) of 10 representative genes of ISCs or ISC subsets [rows]).

(E) MHCII expression in ISCs. Distributions of mean expression levels ($\log_2(\text{TPM} + 1)$, y axis) of MHCII genes (STAR Methods) in each ISC subset and dendritic cells (DC) (Shalek et al., 2014). *** $p < 0.001$, Mann-Whitney U test.

(F) Enriched MHCII gene expression in ISCs. Relative mean expression (row-wise Z score of $\log_2(\text{TPM} + 1)$ values, color bar) of MHCII-related genes (rows) in each IEC type (columns). EP, enterocyte progenitor; EEC, enteroendocrine cell.

(G) MHCII expression *in situ*. IFA co-stain of MHCII (I-A/I-E; green) and the Paneth cell marker Lyz1 (red) in intestinal crypts of WT (top) and MHCII KO (bottom) mice. Yellow arrows, MHCII-expressing cells. Scale bar, 20 μm .

See also Figures S1 and S2 and Tables S1 and S2.

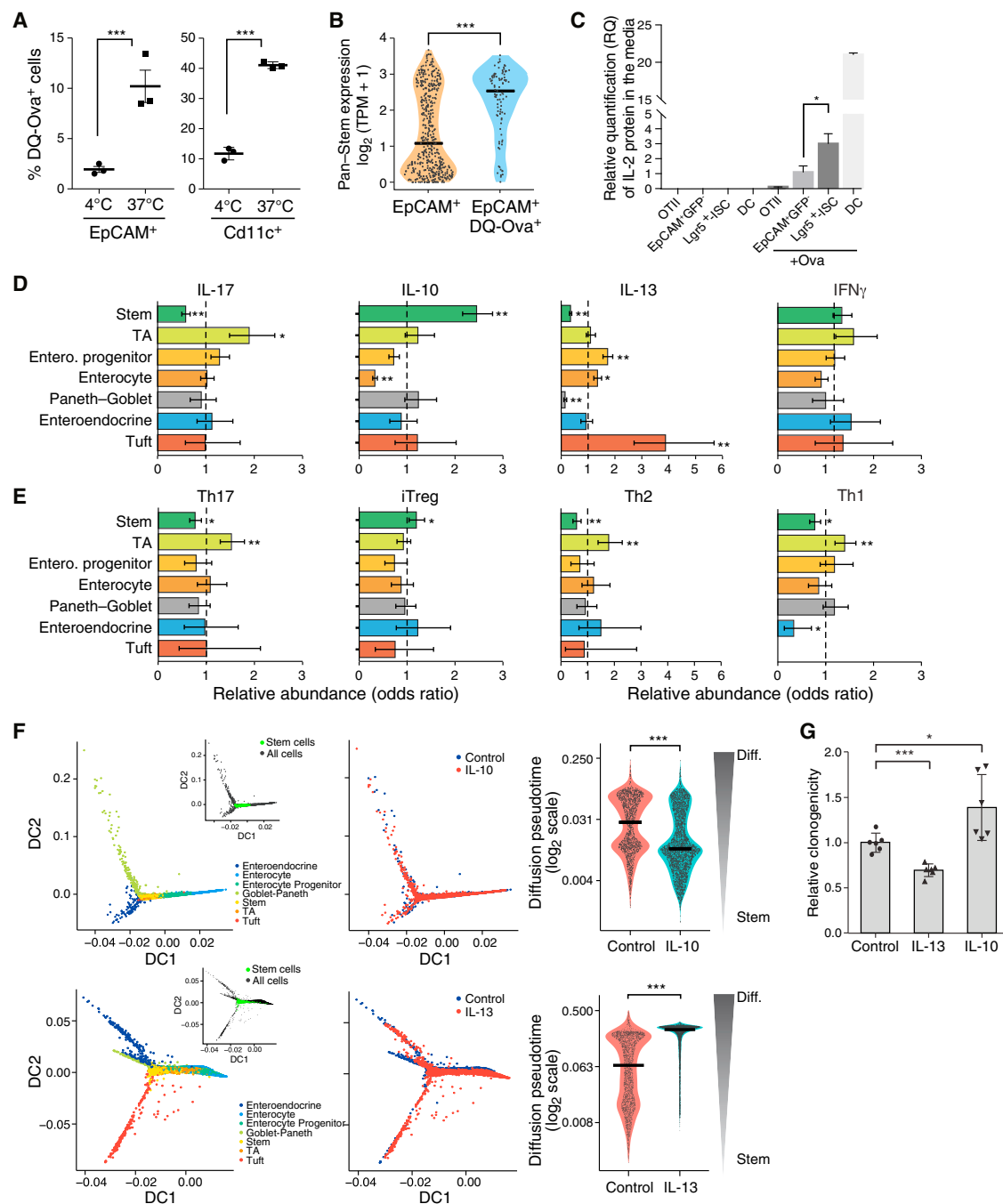


Figure 2. Antigen Presentation by ISCs and the Impact of Th Cytokines on IEC Differentiation

(A) IECs process ovalbumin antigen. Proportion of cells positive for DQ-ovalbumin (DQ-Ova) (y axis) among EpCAM⁺ cells (left) and DCs (right) incubated with 10 μ g of DQ-Ova (x axis). n = 3 mice, ***p < 0.01, t test; error bars, SEM.

(B) DQ-Ova⁺ IECs are enriched for ISCs. Distribution of ISC signature scores in scRNA-seq of EpCAM⁺ or EpCAM⁺ DQ-Ova⁺ cells (**p < 0.001, Wilcoxon test). (C) Lgr5⁺ ISCs interact with and activate naive Th cells. Relative quantification (RQ) of IL-2 secreted in the media (y axis) of naive OTII cells cultured alone or with EpCAM⁺ GFP⁻, EpCAM⁺ GFP⁺ (Lgr5⁺ ISC) or DCs with or without 15 μ g/mL Ova peptide (n = 9 mice, *p < 0.05, t test; error bars, SEM). All groups were compared to EpCAM⁺ GFP⁻ + Ova group.

(D and E) Changes in IEC composition in organoids treated with cytokines (D) or co-cultured with polarized Th cells (E). Relative abundance (odds ratio, y axis) of each IEC-type (by clustering, STAR Methods) under each condition versus their proportions in control organoids (dashed line). *p < 0.01, **p < 10⁻⁴ (hypergeometric test; error bars, 95% confidence interval for the odds ratio).

(legend continued on next page)

differentiation yielded <20% IL-4- and IL-13-expressing cells, while other Th subsets had higher differentiation rates (data not shown). There are also differences between organoids and IECs: goblet and Paneth lineages do not fully diverge (Figure S3F), as we also observed in another organoid scRNA-seq dataset (Grün et al., 2015) (data not shown).

Both co-culture with iT_{regs} and stimulation with IL-10 led to ISC expansion within organoids, while co-cultures with Th1, Th2, and Th17 cells or treatment with IL-13 or IL-17 all decreased the ISC pool based on clustering (Figures 2D, 2E, and S3G–S3I; Table S3). This effect was highlighted along the stem cell differentiation continuum by diffusion maps (Haghverdi et al., 2015): cells from IL-10-treated organoids had a significantly more “stem-like” pseudotime distribution, while cells from IL-13-treated organoids showed the opposite effect (Figure 2F). IL-22 treatment increased enterocyte numbers and organoid growth (data not shown), as shown previously (Lindemans et al., 2015) and distinct from IL-10’s effect.

Consistent with their depleted stem cell pool, organoids co-cultured with Th1, Th2, or Th17 cells or treated with IL-17a had expanded numbers of transit amplifying (TA) cells (Figures 2D and 2E). MHCII was elevated in IECs in Th1 co-cultures (Figure S3C). However, at the low concentration of IFN γ (0.5 u/mL) we used to avoid organoid apoptosis (Farin et al., 2014), we did not observe the expected upregulation of MHCII genes. IL-13 treatment decreased the proportion of secretory “Paneth-goblet” cells and increased tuft cells, as previously described (Gerbe et al., 2016; Howitt et al., 2016; von Moltke et al., 2016) (Figures 2D, 2F, S3J, and S3K), and Th1 co-culture upregulated Paneth cell-specific genes (Figures 2E, S3K, and S3L).

The effects of Th cytokines on the ISC pool suggest that they modulate ISC renewal potential (Figures 2D–2F), which in turn should affect the ability of ISCs to form organoid cultures. To test this, we measured how many organoids grew 3 days after re-seeding of equal numbers of cytokine-treated organoids (n = 6 per group, STAR Methods) (Beyaz et al., 2016). We observed a significant reduction in the clonogenicity of organoids treated with IL-13, whereas IL-10 induced higher clonogenicity (Figure 2G), confirming that Th cytokines impact ISC renewal.

The ISC Pool Expands when MHCII Is Genetically Ablated in Epithelial Cells *In Vivo*

To assess the role of MHCII in IECs under homeostatic conditions *in vivo*, we next examined a MHCII conditional KO model. We crossed H2-Ab1^{f/f} mice (Hashimoto et al., 2002) to Villin-Cre-ERT2 mice (el Marjou et al., 2004), generating a mouse model of specific and inducible MHCII KO in IECs (MHCII^{Δgut}, STAR Methods). We profiled 1,559 MHCII^{Δgut} IECs and 1,617 MHCII^{f/f} IECs (n = 5 mice per group) 10 days post-tamoxifen (Tam) induction. We validated MHCII ablation in IECs (Figures

3A and S4A), but not in DCs of the mesenteric lymph node and LP (Figure S4B and data not shown).

Clustering revealed a 17.6% increase in ISCs proportion in MHCII^{Δgut} mice (Figures 3C, S4D, and S4E). Moreover, there was a 30.3% increase in Lgr5-expressing cells in MHCII^{Δgut} mice by scRNA-seq (Figure S4C), which we confirmed with Lgr5 and Olfm4 *in situ* (Figure 3B and data not shown). Consistently, ISC markers were overrepresented among the genes upregulated in cells from MHCII^{Δgut} mice (Figure S4F). Within all ISCs from MHCII^{Δgut} mice, the proportion of ISC-II cells was significantly higher, while that of ISC-III cells was significantly lower (Figure 3D). Importantly, there was a reduction in CD4 $^+$ cells in the crypt LP of MHCII^{Δgut} mice (Figure 3E), while the number of CD4 $^+$ cells in the villus LP was unchanged (Figure S4G).

We also confirmed this effect in Lgr5 $^+$ ISC-specific inducible MHCII KO mice (MHCII^{ΔISC}, STAR Methods) generated by crossing Lgr5-GFP mice with H2-Ab1^{f/f} mice. Ten days post-Tam treatment resulted in ablation of MHCII in Lgr5 GFP $^+$ ISCs and their progeny tested by IFA (Figure 3F) and flow cytometry, while CD11c $^+$ cells from the LP retained MHCII expression (data not shown). Lgr5 $^+$ ISCs were expanded in MHCII^{ΔISC} mice based on FACS and IFA of Lgr5 GFP $^+$ ISCs (Figures 3G, 3H, and S4H, n = 5 mice). Co-culture with Lgr5 $^+$ ISCs from MHCII^{ΔISC} did not activate naive OTII cells in the presence of Ova peptide, in contrast to robust activation by MHCII-proficient Lgr5 $^+$ ISCs (Figures 3I and S3A). These results indicate that ablation of MHCII in IECs in general (MHCII^{Δgut}) or in Lgr5 $^+$ ISCs specifically (MHCII^{ΔISC}) eliminated the ability of ISCs to activate T cells in co-culture and increased Lgr5 $^+$ ISC numbers and the expression of ISC markers.

MHCII $^+$ Lgr5 $^+$ ISCs Are Involved in IEC Remodeling during Infection

To examine IEC remodeling *in vivo*, we next analyzed scRNA-seq data of 9,842 IECs (Haber et al., 2017) and 5,122 CD45 $^+$ immune cells (STAR Methods) from mice infected with *Salmonella enterica* (*Salmonella*) or *Heligmosomoides polygyrus* (*H. polygyrus*) (Haber et al., 2017). As expected, *Salmonella* induced Th1 responses (Figures S5A–S5C; Table S4) and an increase in Paneth cell numbers, while *H. polygyrus* caused tuft cell expansion (Haber et al., 2017) (Figures S5D and S5E). There was a mild reduction in the expression of a pan-stem signature (Figures 4A and S5F), but a substantial increase in MHCII expression (Figures 4B and S5F) and a shift in the relative proportions of the three ISC subsets (Figures 4C and S5G), with reduction in cells expressing the ISC-I program and elevation of those expressing the ISC-II and -III programs (Figures 4C and 4D).

We next assessed the role of MHCII in ISC differentiation by concurrently infecting mice with *H. polygyrus* for 3 days and treating them with either MHCII-blocking (α -MHCII) or control

(F) IL-10 reduces and IL-13 increases ISC differentiation in organoids. Left and middle: diffusion maps for control and IL-10 (top) or IL-13 (bottom) treated organoids. Cells (points) colored by type (left inset: stem cells) or condition (middle). Right: distribution of cells (points) along the differentiation pseudotime (STAR Methods). ***p < 10⁻⁵, Mann-Whitney U test.

(G) Cytokine pre-treatment alters clonogenicity. Relative clonogenicity of organoid cultures (y axis) of equal organoids number re-seeded post-IL-10 or -IL-13 treatment (x axis). Dots: technical replicates. Error bars: SD, *p < 0.05, ***p < 0.0005, t test.

See also Figure S3 and Table S3.

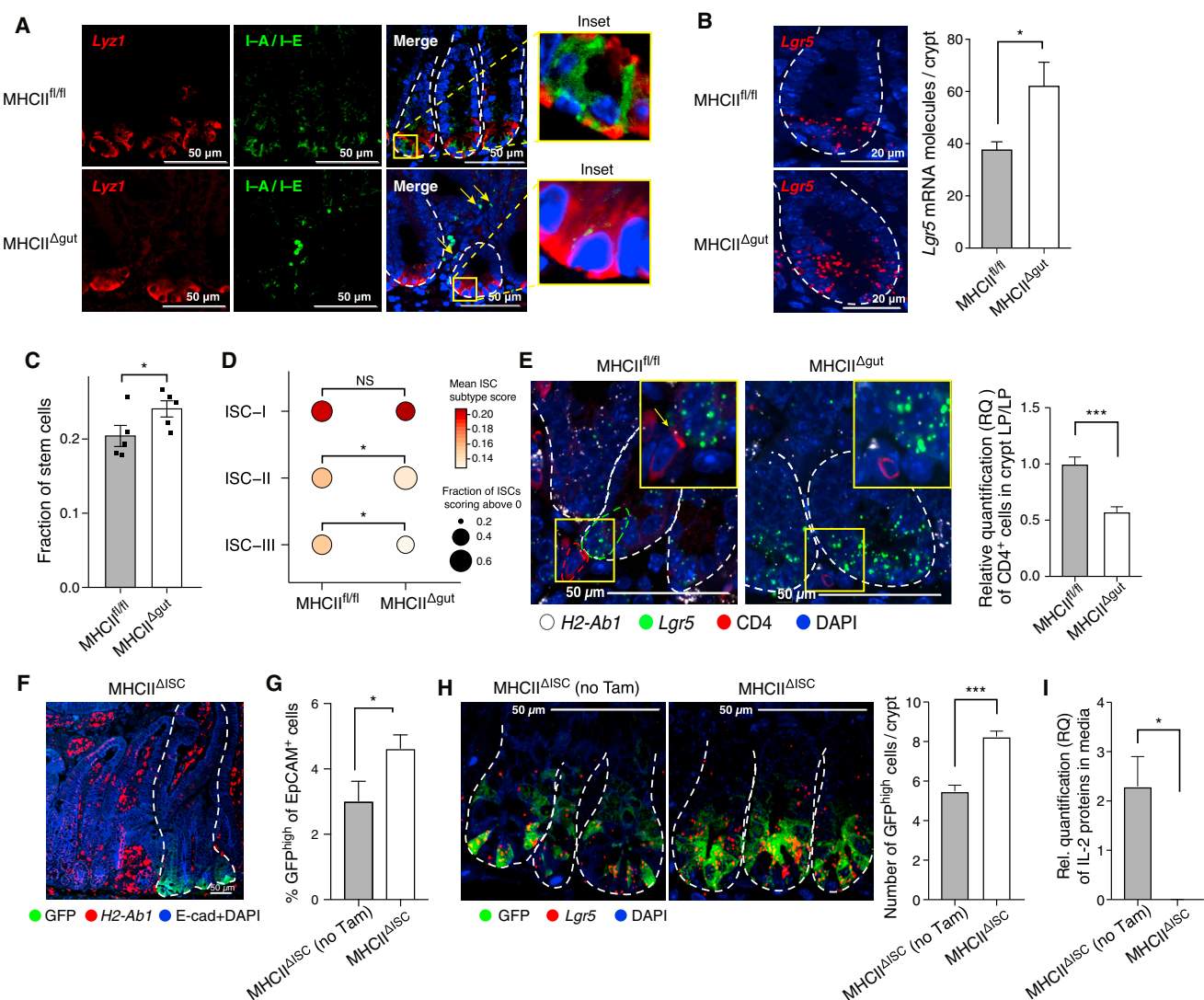


Figure 3. Lgr5⁺ ISC Pool Expands following Epithelial-Specific Ablation of MHCII

- (A) MHCII expression in IECs of MHCII^{Δgut} mouse. IFA of Lyz1 (red) and MHCII (I-A/I-E, green). Inset: $\times 5$ magnification. Yellow arrows: MHCII⁺ cells in LP. Scale bar, 50 μ m.
- (B) Increased Lgr5 expression in crypts of MHCII^{Δgut} mice. Representative single molecule FISH (smFISH, left) and quantification (right) of Lgr5 expression (red) within intestinal crypts of MHCII^{fl/fl} and MHCII^{Δgut} mice. Scale bar, 20 μ M. n = 2 mice, 8 fields per mouse. Error bars: SEM (*p < 0.05, t test).
- (C) Increased ISC pool in MHCII^{Δgut} mice. Fraction of ISCs out of EpCAM⁺ cells (y axis, from scRNA-seq clustering) in MHCII^{fl/fl} and MHCII^{Δgut} mice (points, x axis). Error bars, SEM (*false discovery rate [FDR] <0.05, likelihood-ratio test).
- (D) Decreased ISC-II and -III scores in MHCII^{Δgut} mice. Fraction of ISCs expressing a signature (circle size) and the signature's mean score in those expressing cells (color bar) for each ISC subset signature (rows) in each genotype (columns). *p < 0.05, Mann-Whitney U test.
- (E) Th cell number reduction in crypt LP of MHCII^{Δgut} mice. Combined smFISH and IFA of small intestine from MHCII^{fl/fl} and MHCII^{Δgut} mice. Left: representative images; yellow arrow: CD4⁺ cell adjacent to Lgr5⁺ ISCs; scale bar, 50 μ m. Inset: $\times 3$ magnification. Right: relative quantification (RQ, y axis) of the number of CD4⁺ cells per crypt LP/total LP. n = 3 mice, 8 fields per mouse (**p < 0.0001, t test; error bars, SEM).
- (F) H2-Ab1 is deleted in GFP⁺Lgr5⁺ ISCs and their progeny. Combined smFISH and IFA in IECs emerging from GFP labeled crypts (dashed line) versus non-labeled crypts. High expression of H2-Ab1 is found in both the non-labeled crypts and in the LP. Scale bar, 50 μ m.
- (G and H) Increased Lgr5⁺ ISC fraction in MHCII^{ΔISC}.
- (G) Bar plot of the percentage (y axis, by FACS, see also Figure S4H) of GFP^{high} cells in MHCII^{ΔISC} or matching non-tamoxifen induced controls (MHCII^{ΔISC} [no Tam]). n = 5 mice, *p < 0.015, t test; error bars, SEM.
- (H) Combined smFISH and IFA of 10 days tamoxifen (MHCII^{ΔISC}) and non-tamoxifen (MHCII^{ΔISC} [no Tam])-induced mice. Left: representative images; scale bar, 50 μ m. Right: number of Lgr5⁺ ISCs (GFP^{high}) per crypt (y axis). n = 3 mice, 8 fields per mouse (**p < 0.0001, t test; error bars, SEM).
- (I) Lgr5⁺ ISCs of MHCII^{ΔISC} mice do not activate naive Th cells in co-culture. IL-2 secreted in the media (RQ, y axis) of naive OTII cells cultured with Lgr5⁺ ISCs from MHCII^{ΔISC} or non-tamoxifen MHCII^{ΔISC} controls (no Tam) in presence of 15 μ g/mL Ova peptide (n = 3 mice, *p < 0.05, t test; error bars, SEM). Each group was compared to the EpCAM⁺GFP⁻ group (as in Figure 2C).

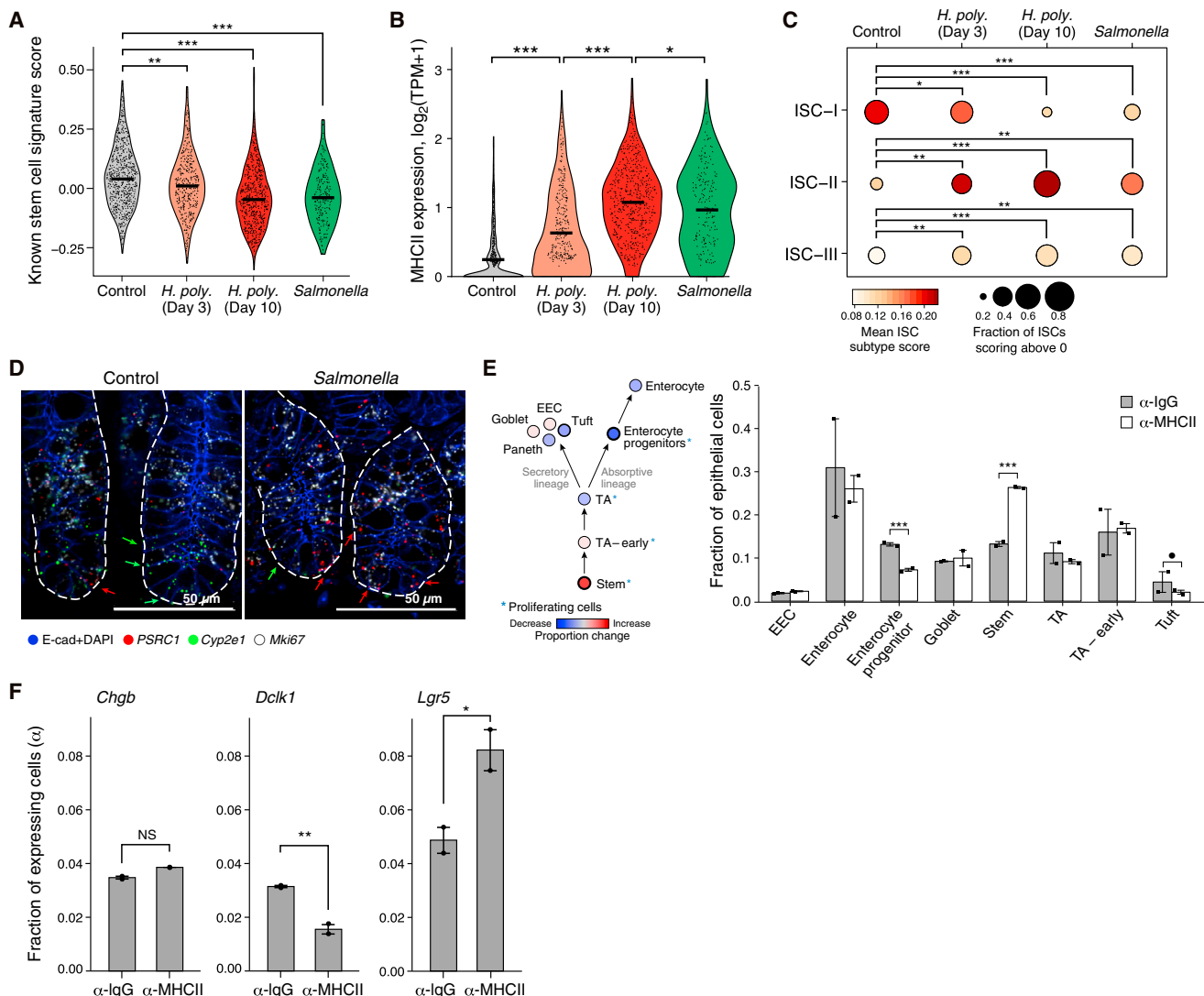


Figure 4. IEC Remodeling under Pathogenic Infection Driven by Shifts in ISC Subsets

(A and B) Reduced stemness and increased MHCII expression scores in ISCs during pathogenic infection. Distribution of stemness signature (A) and MHCII expression (B) scores (y axis) in 1,857 ISCs from scRNA-seq (Haber et al., 2017). **p < 0.01, ***p < 10⁻⁵ (Mann-Whitney U test).

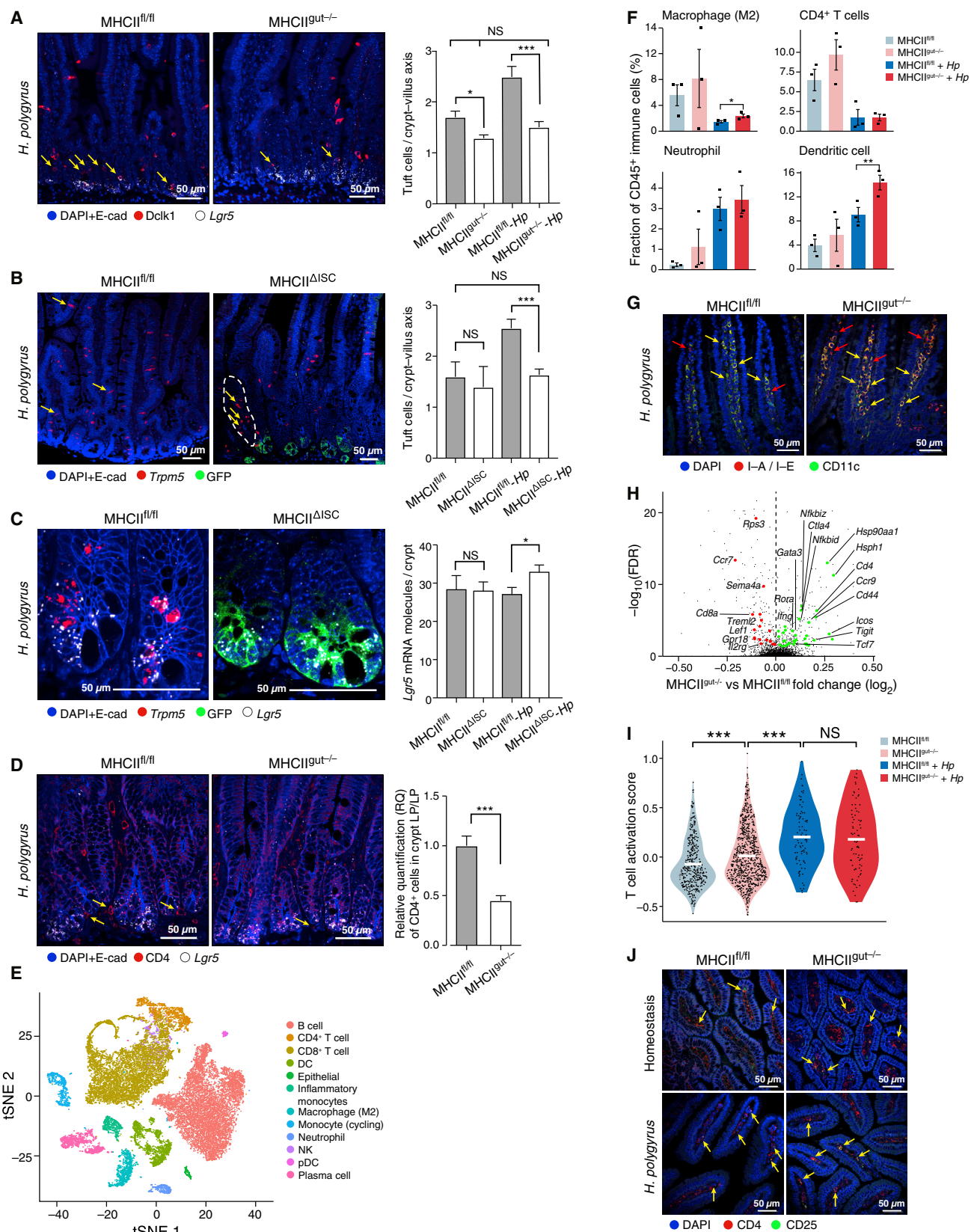
(C and D) Shifts in ISC subsets under infection. (C) Fraction of ISCs expressing a signature (circle size) and the signature's mean score in those expressing cells (color bar) for each ISC subset signature (rows) in each condition (columns). *p < 0.001, **p < 10⁻⁵, ***p < 10⁻¹⁰, Mann-Whitney U test. (D) Combined smFISH and IFA of crypts at homeostasis (left) and 2 days post-infection (right). Green arrow, Cyp2e1⁺ cell; red arrow, PSRC1⁺ cell; scale bar, 50 μm. Cyp2e1: ISC-I marker (green), *Psarc1*: ISC-III marker (red).

(E) α-MHCII leads to changes in cell proportions. Right: frequencies (y axis, unsupervised clustering) of each cell subtype (x axis) in mice infected with *H. polygyrus* and treated with either α-MHCII (white bars) or with α-IgG (gray bars). ***p < 10⁻¹⁰ (likelihood-ratio test). Left: schematic summary of changes in cell proportions in each cell type (node) (red, increase; blue, decrease; scale bar, bottom). Bold outline: statistically significant; *proliferating cells. ·p < 0.1; error bars, SEM.

(F) Reduction in tuft cell and increase in Lgr5⁺ ISC proportions following α-MHCII during *H. polygyrus* infection. Frequency of cells expressing *Chgb*, *Dclk1*, or *Lgr5* by scRNA-seq (y axis) 3 days post-infection and treated with either α-IgG or α-MHCII (x axis). *FDR < 0.1, **FDR < 0.01 (likelihood-ratio test). Error bars, SEM. See also Figure S5.

anti-IgG (α -IgG) antibodies, followed by scRNA-seq and cell-type identification (Figure 4E). Compared to α -IgG treated control, mice treated with α -MHCII showed reduced tuft cell proportions post-infection and increased ISC proportions (Figures 4E and 4F). This experiment, however, cannot exclude indirect effects of α -MHCII, such as impacting APCs directly, which in turn affect Th2 differentiation (Ziegler and Artis, 2010).

We therefore tested the impact of MHCII deletion in IECs during *H. polygyrus* infection, using either a constitutive epithelial H2-Ab1 KO driven by the Villin promoter (Madison et al., 2002) (MHCII^{gut-/-}, STAR Methods) or the MHCII^{ΔISC} model. For MHCII^{ΔISC}, to minimize indirect effects, we induced the conditional KO shortly before infection (6 days). There was little or no tuft cell expansion in both mouse models 4 days



(legend on next page)

($\text{MHCII}^{\text{gut}--}$) or 10 days ($\text{MHCII}^{\Delta\text{ISC}}$) post-infection, in marked contrast to the expansion in infected matched controls (Figures 5A–5C). Conversely, *Lgr5* expression was upregulated in $\text{MHCII}^{\Delta\text{ISC}}$ mice during infection compared to $\text{MHCII}^{\text{fl}/\text{fl}}$ controls (Figure 5C). Importantly, $\text{MHCII}^{\text{gut}--}$ mice infected with 200 *H. polygyrus* larvae had higher worm burden compared to $\text{MHCII}^{\text{fl}/\text{fl}}$ controls after 6 weeks of infection (66 ± 12.46 versus 16.17 ± 5.94 worms/mouse [mean \pm SD]; $n = 6$ mice/group; $p < 0.005$, t test).

MHCII Deletion in the Epithelial Compartment Activates the Local Immune System

The immune compartment—especially DCs and Th cells—was substantially modulated in both homeostasis and *H. polygyrus* infection after MHCII ablation in IECs (Figures 5D–5J). We performed scRNA-Seq of CD45⁺ cells from the LP of $\text{MHCII}^{\text{gut}--}$ and $\text{MHCII}^{\text{fl}/\text{fl}}$ mice, at homeostasis and 4 days post-infection ($n = 3$ in each group, 24,649 cells overall, Figure 5E), and tested immune cell markers *in situ*. (Due to the mosaic nature of $\text{MHCII}^{\Delta\text{ISC}}$, we did not profile their immune cells.) First, during infection, only macrophage and DC proportions were significantly affected by IEC-MHCII deletion (Figures 5F and 5G), with a particularly strong increase (61.6%) in DCs in $\text{MHCII}^{\text{gut}--}$ post-infection (but not at baseline). Second, although overall Th cell proportions were not affected by the KO in either infection or homeostasis (Figure 5F), Th cells from uninfected $\text{MHCII}^{\text{gut}--}$ mice expressed higher levels of a T cell activation signature compared to controls (Figures 5H and 5I; Table S5; STAR Methods). This signature was further increased to comparable levels in both $\text{MHCII}^{\text{fl}/\text{fl}}$ and $\text{MHCII}^{\text{gut}--}$ mice upon infection (Figures 5I and 5J). Finally, there was a strong reduction in the number of CD4⁺ cells found in close proximity to Lgr5⁺ ISCs in $\text{MHCII}^{\text{gut}--}$ mice following *H. polygyrus* infection by IFA, a reduction also observed in uninfected $\text{MHCII}^{\Delta\text{gut}}$ mice (Figures 3E and S4G). Conversely, villus CD4⁺ cell numbers were not

affected by the KO (Figure 5D and data not shown). These results suggest that MHCII expression by epithelial cells impacts both the innate and adaptive responses, some of which may propagate indirect effects, for example dendritic cells during infection.

The ISC Pool Increases in T Cell-Depleted Mice

To examine the role of T cells in Lgr5⁺ ISC differentiation axis, we next assessed two T cell-deficient mouse models. We profiled 2,967 IECs from athymic B6 nude mice (Cordier and Haumont, 1980) ($n = 2$), characterized by T cell depletion. Clustering revealed significantly higher fractions of ISCs (52.5% increase, STAR Methods), TA, and enteroendocrine cells compared to control mice ($n = 6$, Figures S6A and S6B) and a decrease in enterocyte progenitors. Consistently, ISC markers were enriched (56 of 1,804 genes) (Figure S6A; Table S6) among genes overall upregulated in cells of nude versus controls. Similar analysis of 9,488 IEC profiles from TCRβ KO mice ($n = 2$) (Mombaerts et al., 1992), which lack α/β T cells, also showed a significant expansion of the ISC pool (35.0% increase) (Figures S6C and S6D) and a decrease in enterocyte progenitors (as well as an increase in goblet cells). We confirmed the increased expression of *Lgr5* mRNA *in situ* (Figure S6E). Thus, T cell (or only α/β T cells) ablation leads to ISCs accumulation, possibly due to diminished differentiation capacity, in particular toward the absorptive lineage.

T_{reg}s Help Maintain the Lgr5⁺ ISC Niche In Vivo

In our organoid assays, only T_{reg} cells and their key cytokine IL-10 promoted renewal of the ISC pool. To confirm this *in vivo*, we used Foxp3-DTR mice (Kim et al., 2007), in which T_{reg}s are depleted upon administration of diphtheria toxin (DT). Foxp3⁺ T_{reg}s are the major source of IL10 expression based on our LP scRNA-seq (data not shown). To minimize indirect effects, we induced T_{reg} depletion with DT for only 4 or 7 days (Chinen et al., 2010; Kim et al., 2007). We confirmed T_{reg} ablation in the

Figure 5. Deletion of Epithelial MHCII Disrupts Mucosal Immune Responses

(A and B) *H. polygyrus*-induced tuft cell hyperplasia is abolished in IEC-MHCII KO mice. Left: representative images of combined smFISH and IFA of proximal SI from $\text{MHCII}^{\text{fl}/\text{fl}}$ and $\text{MHCII}^{\text{gut}--}$ (A) or $\text{MHCII}^{\text{fl}/\text{fl}}$ and $\text{MHCII}^{\Delta\text{ISC}}$ (B) at 4 days (A) or 10 days (B) post-infection. (A) Scale bar, 50 μm . Yellow arrows, Dclk1⁺ cells emerging from the crypt. (B) Scale bar, 50 μm . Yellow arrows, mature *Trpm5*⁺ villus tuft cells. Dashed line: a crypt in which GFP is absent and ISC^{fl/fl} reside due to the mosaic knockout in $\text{MHCII}^{\Delta\text{ISC}}$. This crypt-villus axis is associated with higher tuft cell numbers. Right: number of Dclk1⁺ (A) or *Trpm5*⁺ (B) tuft cells per crypt-villus axis (y axis). $n = 3$ (A) or 4 (B) mice per group, 10 fields per mouse (NS, not significant, * $p < 0.05$, ** $p < 0.0001$, t test; error bars, SEM).

(C) *H. polygyrus* infection increases *Lgr5* expression in $\text{MHCII}^{\Delta\text{ISC}}$ mice. Left: representative images of combined smFISH and IFA of proximal SI from $\text{MHCII}^{\text{fl}/\text{fl}}$ and $\text{MHCII}^{\Delta\text{ISC}}$ mice 10 days post-infection. Scale bar, 50 μm . Right: number of *Lgr5* mRNA molecules per crypt (y axis). $n = 4$ mice, 10 fields per mouse (NS, not significant, * $p < 0.05$, t test; error bars, SEM).

(D) Reduced number of crypt Th cells in $\text{MHCII}^{\text{gut}--}$ mice 4 days post-infection. Left: representative images from combined smFISH and IFA of SI from $\text{MHCII}^{\text{fl}/\text{fl}}$ and $\text{MHCII}^{\text{gut}--}$ mice. Scale bar, 50 μm . Yellow arrows, CD4⁺ cells in close proximity to Lgr5⁺ cells. Right: relative quantification (RQ) of CD4⁺ cells per crypt LP/total LP (y axis). $n = 3$ mice per genotype, 10 fields per mouse (** $p < 0.0001$, t test; error bars, SEM).

(E) LP immune cell types by scRNA-seq. tSNE of 24,649 CD45⁺ LP cells at homeostasis and 4 days post-infection ($n = 12$ mice), colored by clustering and annotated post hoc (STAR Methods).

(F and G) Increased APC proportions in $\text{MHCII}^{\text{gut}--}$ mice 4 days post-infection. (F) Fraction of immune subsets by clustering (from E, y axis) of $\text{MHCII}^{\text{fl}/\text{fl}}$ and $\text{MHCII}^{\text{gut}--}$ mice (points) at homeostasis and 4 days post-infection (x axis, color code). Error bars, SEM (*FDR < 0.05, **FDR < 0.005, likelihood-ratio test). (G) Representative IFA images of SI from $\text{MHCII}^{\text{fl}/\text{fl}}$ and $\text{MHCII}^{\text{gut}--}$ 4 days post-infection. Scale bar, 50 μm . Yellow arrows, double positive cells; red arrows, CD11c⁺ MHCII⁺ cells.

(H–J) Increased Th cell activation in $\text{MHCII}^{\text{gut}--}$ at homeostasis. (H) Mean log₂ fold-change (x axis) and significance (-log₁₀(FDR)) of DE genes between Th cells of $\text{MHCII}^{\text{gut}--}$ mice (765 cells, $n = 3$ mice) and $\text{MHCII}^{\text{fl}/\text{fl}}$ controls (385 cells, $n = 3$ mice) at homeostasis. Green/red dots, up/downregulated Th cell activation genes (FDR < 0.05, likelihood-ratio test). (I) Distribution of Th cell activation signature scores (y axis) in 1,319 cells from $\text{MHCII}^{\text{gut}--}$ (846 cells, $n = 3$ mice) and $\text{MHCII}^{\text{fl}/\text{fl}}$ controls (473 cells, $n = 3$ mice) at homeostasis and 4 days post-infection (color legend). White bars, mean. *** $p < 10^{-5}$; NS, not significant, Mann-Whitney U test. (J) Representative images of IFA of SI villi of $\text{MHCII}^{\text{fl}/\text{fl}}$ and $\text{MHCII}^{\text{gut}--}$ mice at homeostasis (top) and 4 days post-infection (bottom). Scale bar, 50 μm . Arrow, CD25⁺ CD4⁺ cell.

See also Table S5.

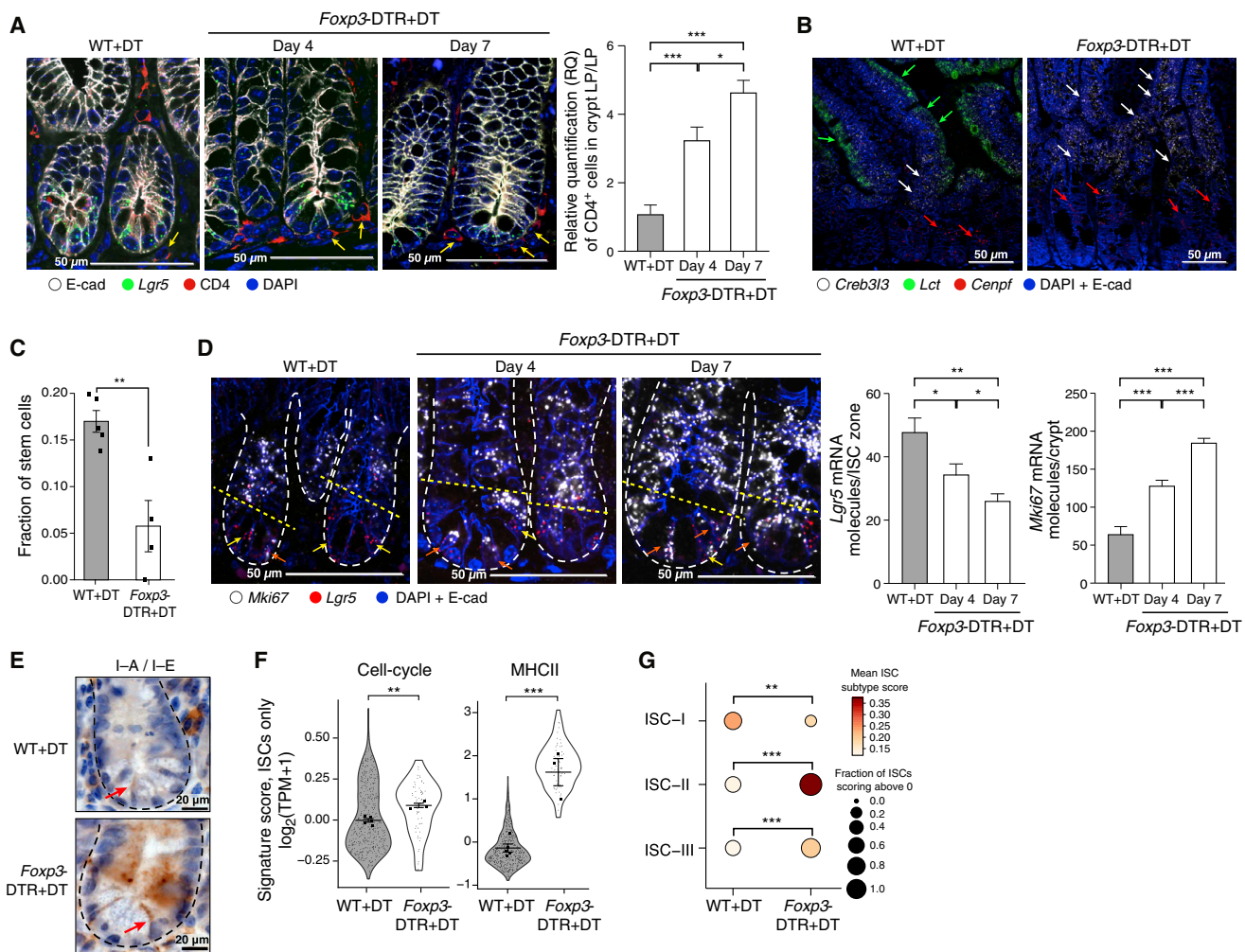


Figure 6. T_{reg} Ablation Decreases the Lgr5⁺ ISC Pool

- (A) Increase in CD4⁺ cells in T_{reg} ablated crypts. Combined smFISH and IFA of SI from WT or *Foxp3*-DTR mice treated with diphtheria toxin (DT) for 4 or 7 days. Left: representative images. Arrows, CD4⁺ cells adjacent to Lgr5⁺ ISCs. Scale bar, 50 μ m. Right: relative quantification (RQ) of CD4⁺ cells per crypt LP/total LP (y axis). n = 2 mice, 8 fields per mouse per time point (*p < 0.02, **p < 0.0003, t test; error bars, SEM).
- (B) Depletion of mature enterocytes post-T_{reg} ablation. Combined IFA and smFISH of SI in WT and *Foxp3*-DTR mice treated with DT. Lct: mature enterocyte marker, *Crebl3l3*, *Cenpf*: early enterocyte markers (Haber et al., 2017). Green, red, white arrows: Lct⁺, *Cenpf*⁺, and *Crebl3l3*⁺ cells, respectively. Scale bar, 50 μ m.
- (C) Reduction in ISC numbers following T_{reg} ablation. Fraction of ISCs among EpCAM⁺ cells (y axis, by clustering) in WT and *Foxp3*-DTR mice 7 days post-DT treatment. Error bars, SEM (**FDR < 0.005, likelihood-ratio test, STAR Methods).
- (D) Reduced Lgr5 expression and increased cell proliferation following T_{reg} ablation. Combined smFISH and IFA of SI from WT and *Foxp3*-DTR mice treated with DT for 4 or 7 days. Left: representative images. Yellow arrows, *Mki67*⁻ Lgr5⁺ ISCs; orange arrows, *Mki67*⁺ Lgr5⁺ ISCs. Scale bar, 50 μ m. Right: number of Lgr5 (mid-right) and *Mki67* (right) molecules per crypt (y-axes). n = 2 mice, 8 fields per mouse per time point (*p < 0.05, **p < 0.001, ***p < 0.0001 t test; error bars, SEM).
- (E and F) Increased MHCII expression in ISCs of T_{reg}-depleted mice. (E) IHC of MHCII (I-A/I-E; brown) co-stained with hematoxylin (blue) within the intestinal crypt of WT and *Foxp3*-DTR mice treated for 7 days with DT. Arrows, MHCII⁺ Lgr5⁺ ISC. (F) Distribution of the scores for cell cycle (left) and MHCII (right) genes in ISCs from WT (n = 5; 464 cells) and *Foxp3*-DTR (n = 4; 62 cells) mice 7 days post-DT. Squares, mean score per mouse; thick bar, overall mean; error bars, SEM (*p < 0.05, **p < 0.005, ***p < 5 \times 10⁻⁴, likelihood-ratio test).
- (G) Changes in ISC subsets in T_{reg}-depleted mice. Fraction of ISCs expressing a signature (circle size) and the signature's mean score in those expressing cells (color bar) for each ISC subset signature (rows) in each genotype (columns). **p < 10⁻⁵, ***p < 10⁻¹⁰, Mann-Whitney U test.

See also Figures S6 and S7.

LP (Figure S7A) and observed higher proliferation rates, including ISCs, and no signs of increased cell death or major gut inflammation in intestinal crypts of *Foxp3*-DTR versus control mice (Figures S7B and S7C). However, Th cell numbers in both the mesenteric lymph nodes and LP were elevated after DT induction (Figures S7D and S7E) and, in particular, at intestinal

crypts in close proximity to Lgr5⁺ ISCs (Figures 6A and S7E). Overall, this shows that T_{reg} ablation for 4 and 7 days precedes apparent tissue damage. Next, we profiled 3,387 IECs from day 7 *Foxp3*-DTR (n = 4) and matched control (n = 5) mice treated with DT. Consistent with our hypothesis, IEC differentiation was aberrant, with a substantial increase in enterocyte progenitors,

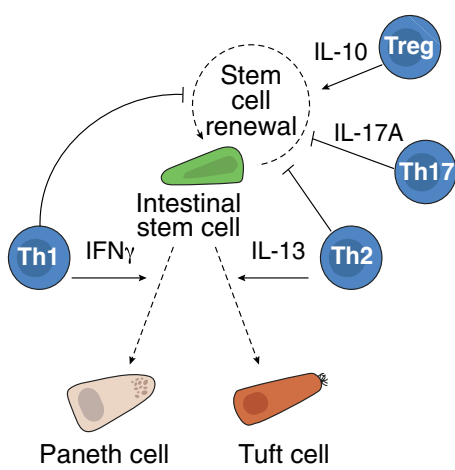


Figure 7. A Model of the Cross-Talk between Th Cells and ISCs

Th subsets (blue nodes) modulate (solid arrows) the fate (dashed arrows) of Lgr5⁺ ISCs (green). T_{regs} and their key cytokine IL-10 promote stem cell renewal, while Th17 cells and their cytokine IL-17a reduce stem cell renewal and promote differentiation. Both Th1 and Th2 (and their cytokines) suppress stem cell renewal and promote specific differentiation toward Paneth cells (tan) and tuft cells (orange), respectively.

tuft, and goblet cells, and reduction in mature enterocytes, by both scRNA-seq and IFA (Figures 6B, S7F, and S7G).

Importantly, Lgr5⁺ ISC proportions were significantly reduced by several measures: (1) clustering of scRNA-seq from day 7 (66.3% decrease) (Figures 6C and S7F), (2) Lgr5 *in situ* stain (Figure 6D), (3) fraction of Lgr5⁺ cells in scRNA-seq data (Figure S7H), and (4) over-representation of ISC genes among those downregulated in T_{reg}-depleted mice (Figure S7I). In addition, ISCs showed elevated MHCII expression (Figures 6E and 6F) and increased proliferation by Ki67 staining and expression of a cell-cycle signature (Figures 6D, 6F, and S7B) and an elevated proportion of MHCII⁺, proliferative ISC-II and -IIIs compared to reduction in the low-cycling MHCII- ISC-I (Figures 6F and 6G). The reduction in ISCs and a shift toward more MHCII⁺ proliferative ISCs in Foxp3-DTR mice supports a model of higher differentiation rates and stem cell pool depletion.

DISCUSSION

Previous studies of stem cell dynamics and differentiation focused on epithelial and stromal signals (Sato et al., 2011; Stappenbeck and Miyoshi, 2009). Here, we used scRNA-seq to uncover interactions between Lgr5⁺ ISCs and the Th cells and their effect on IEC remodeling.

Our results support a model of crosstalk between Th cells and Lgr5⁺ ISCs in which Th cells or their key cytokines interact with Lgr5⁺ ISCs and subsequently impact the ISC pool and modulate its differentiation (Figure 7). In this model, T_{regs} and their key cytokine IL-10 help maintain the Lgr5⁺ ISC niche in the small intestine. T_{reg} ablation resulted in aberrant epithelial cell differentiation: reduction in the Lgr5⁺ ISC pool and accumulation of differentiated cells. This effect might be enhanced by the concomitant increased accumulation of other Th cells (Th1, Th2, and Th17) in the stem cell niche of T_{reg} ablated mice, which

promote Lgr5⁺ ISC differentiation. Indeed, the Lgr5⁺ ISC pool is expanded in pan-T or α/β T cell-depleted mice.

This model can help explain how the ISC pool is maintained during homeostasis and modulated during infection. Upon bacterial or parasite infection, respectively, both Th1 and Th2 cells and their signature IEC-type effects, either increasing Paneth (Th1) or tuft (Th2) cells based on the respective functional demand (e.g., “weep and sweep” for helminth infection) (Anthony et al., 2007). Meanwhile, Th17 cells, reduce the number of Lgr5⁺ ISCs, which may reflect an overall shift toward stem cell differentiation. As T_{regs} are elevated after a strong inflammatory response (Tanoue et al., 2016), they may serve as negative feedback on differentiation to replenish ISC numbers. Additional mouse models, where specific cytokines or immune cells are conditionally depleted, would help elucidate further connections in this ISC-Th cell circuit.

What is the role of the MHCII system in Lgr5⁺ ISCs? First, MHCII⁺ Lgr5⁺ ISC subsets may act as non-conventional APCs and play a role in activating gut-resident Th cells, although further characterization is needed to determine presentation *in vivo*. Microfold (M) cells are the key sentinels of antigen sampling in the small intestine (Mabbott et al., 2013), but are rare and localized to Peyer's patches. Lgr5⁺ ISC-mediated presentation could provide an alternate mechanism by which IECs can sense and initiate a response to signals coming from the lumen. Second, the epithelial MHCII machinery is important to maintain appropriate IEC differentiation, possibly by presentation to and contact with Th cells. Third, the MHCII system may be induced by infections. We observed a shift toward MHCII⁺ Lgr5⁺ ISC states in both bacterial and helminth infection and showed that during *H. polygyrus* infection, MHCII deletion in IECs or Lgr5⁺ ISCs inhibits IEC remodeling, elevates Lgr5⁺ ISC numbers, and enhances infection severity. Thus, ISC-Th interactions via MHCII together with IL-25 mediated tuft-ILC interactions (Howitt et al., 2016; von Moltke et al., 2016) could regulate appropriate host responses against parasites. Moreover, the expression of MHCII genes in IECs is induced by Th1 cells (potent producers of IFNγ) in our organoid co-culture system. Thus, IFNγ-producing cells may play a key role in initiating Th cell-Lgr5⁺ ISC crosstalk. Finally, MHCII expression in IECs may impact the mucosal immune system. Indeed, because deletion of MHCII led to changes in both DC numbers and Th cells activity, some of the observed phenotypes may be indirectly mediated through additional compartments, such as changes in dendritic cells or ISC states (Nusse et al., 2018) and further work, including lineage tracing of ISC subsets, is still needed to clarify the role of epithelial MHCII.

Taken together, the ISC-Th axis may provide a way to integrate epithelial and immune responses to titrate responses to luminal flora and avoid continuous inflammation after infection. Lgr5⁺ ISCs respond to pro- and anti-inflammatory signals to balance between renewal and differentiation, which may boost the desired immune response concordantly with signals arriving from the lumen. It is possible that MHCII expression on stem cells plays a similar role in crosstalk with Th cells in other mucosal or non-mucosal tissues, as a general mechanism by which adaptive immune cells regulate parenchymal stem cells to maintain or restore tissue homeostasis.

STAR★METHODS

Detailed methods are provided in the online version of this paper and include the following:

- **KEY RESOURCES TABLE**
- **CONTACT FOR REAGENT AND RESOURCE SHARING**
- **EXPERIMENTAL MODEL AND SUBJECT DETAILS**
 - Mice
 - Infection models
 - *In vitro* and *ex vivo* cultures
- **METHOD DETAILS**
 - BrdU and EDU incorporation
 - MHCII deletion in intestinal cells
 - *S. enterica* and *H. polygyrus* infection
 - Diphtheria toxin
 - Epithelial cell dissociation and crypt isolation
 - Immune cell isolation
 - Intestinal organoid cultures
 - Antigen processing and presentation
 - Cell sorting
 - Plate-based scRNA-seq
 - Droplet-based scRNA-seq
 - Div-Seq
 - Immunofluorescence and single-molecule fluorescence *in situ* hybridization (smFISH)
 - Image analysis
 - Two-photon intra-vital microscopy (2P-IVM) of T cells and Lgr5⁺ ISCs
- **QUANTIFICATION AND STATISTICAL ANALYSIS**
 - Image quantification
 - Pre-processing of plate-based scRNA-seq data
 - Pre-processing of droplet-based scRNA-seq data
 - Dimensionality reduction by PCA
 - tSNE visualization
 - Removing doublets
 - *k*-NN graph-based clustering
 - Assigning the three Lgr5⁺ISC states to region of origin using supervised classification
 - Cell-cell similarity matrix
 - Cell-cycle and Lgr5⁺ ISC subset signatures
 - Scoring cells using signature gene sets
 - Pseudo-time analysis of stem and progenitor cell differentiation
 - Testing for shifts in cell proportions in intestinal organoids
 - Testing for shifts in cell proportions *in vivo*
 - GO analysis
 - Analysis of CD4⁺ T helper cell activation in MHCII^{gut-/-} mice
- **DATA AND SOFTWARE AVAILABILITY**
 - Additional Resources

SUPPLEMENTAL INFORMATION

Supplemental Information includes seven figures, six tables, and one video and can be found with this article online at <https://doi.org/10.1016/j.cell.2018.10.008>.

ACKNOWLEDGMENTS

We thank Leslie Gaffney and Anna Hupalowska for help with figures, Tim Tickle for help with the Single Cell Portal, Alexandra-Chloe Villani for discussions, the Broad Flow Cytometry Facility (Patricia Rogers, Stephanie Saldi and Chelsea Otis), and the Histology facility at the Koch Institute (Kathleen Cormier, Charlene Condon and Michael Brown). M.B. was supported by a postdoctoral fellowship from the Human Frontiers Science Program. O.H.Y. is the recipient of the Sidney Kimmel Scholar Award, the Pew-Stewart Trust Scholar Award, and is a member in the American Federation of Aging Research. A.S.K. is the recipient of the Pew-Stewart Scholars Program, a Sloan Fellowship in Chemistry, the Searle Scholars Program, and the Beckman Young Investigator Program. Work was supported by the Klarman Cell Observatory (A.R. and R.J.X.), HHMI (A.R.), Broadnext10 (A.R. and R.J.X.), NIH DK043351, DK114784, and DK117263 (R.J.X.), Helmsley Charitable Trust and Crohn's and Colitis Foundation (R.J.X.), NIH CA211184 and AG045144 (O.H.Y.), and NIH New Innovator Award 1DP2OD0 20839 (A.K.S.).

AUTHOR CONTRIBUTIONS

A.R. and R.J.X. supervised this study. M.B. and N.R. carried out all experiments with G.B., S.B., A.S., Z.C., C.W., M.E.X., D.B.G., V.K., and O.H.Y. A.L.H. designed and performed computational analysis with O.A., C.S., K.S., R.H.H., I.T., and A.R. J.O.-M., D.A., A.K.S., and U.H.v.A assisted with intravital imaging. C.-W.S., M.Z., and H.N.S. assisted with pathogen infection. D.D., L.T.N., and O.R.-R. assisted with scRNA-seq. M.B., A.L.H., N.R., A.R., and R.J.X. wrote the manuscript with input from all authors.

DECLARATION OF INTERESTS

A.R. is a SAB member of ThermoFisher Scientific, Syros Pharmaceuticals, and Driver Group. A.R. and R.J.X. are cofounders of Celsius Therapeutics. M.B., A.L.H., N.R., R.H.H., J.O.-M., O.R.-R., A.K.S., K.S., C.S., A.R., and R.J.X. are co-inventors on PCT/US 2014/060469 filed by the Broad Institute relating to innovative advances in modulation of epithelial cells via T cells described in this manuscript.

Received: March 22, 2018

Revised: July 13, 2018

Accepted: October 1, 2018

Published: November 1, 2018

REFERENCES

- Agudo, J., Park, E.S., Rose, S.A., Alibo, E., Sweeney, R., Dhainaut, M., Kobayashi, K.S., Sachidanandam, R., Baccarini, A., Merad, M., et al. (2018). Quiescent tissue stem cells evade immune surveillance. *Immunity* 48, 271–285.
- Ali, N., Zirak, B., Rodriguez, R.S., Pauli, M.L., Truong, H.A., Lai, K., Ahn, R., Corbin, K., Lowe, M.M., Scharschmidt, T.C., et al. (2017). Regulatory T cells in skin facilitate epithelial stem cell differentiation. *Cell* 169, 1119–1129.
- Anthony, R.M., Rutitzky, L.I., Urban, J.F., Jr., Stadecker, M.J., and Gause, W.C. (2007). Protective immune mechanisms in helminth infection. *Nat. Rev. Immunol.* 7, 975–987.
- Arpaia, N., Green, J.A., Moltedo, B., Arvey, A., Hemmers, S., Yuan, S., Treuting, P.M., and Rudensky, A.Y. (2015). A distinct function of regulatory T cells in tissue protection. *Cell* 162, 1078–1089.
- Aurora, A.B., and Olson, E.N. (2014). Immune modulation of stem cells and regeneration. *Cell Stem Cell* 15, 14–25.
- Barker, N., van Es, J.H., Kuipers, J., Kujala, P., van den Born, M., Cozijnsen, M., Haegebarth, A., Korving, J., Begthel, H., Peters, P.J., and Clevers, H. (2007). Identification of stem cells in small intestine and colon by marker gene Lgr5. *Nature* 449, 1003–1007.
- Beyaz, S., Mana, M.D., Roper, J., Kedrin, D., Saadatpour, A., Hong, S.J., Bauer-Rowe, K.E., Xifaras, M.E., Akkad, A., Arias, E., et al. (2016). High-fat diet

- enhances stemness and tumorigenicity of intestinal progenitors. *Nature* 531, 53–58.
- Biton, M., Levin, A., Slyper, M., Alkalay, I., Horwitz, E., Mor, H., Kredo-Russo, S., Avnit-Sagi, T., Cojocaru, G., Zreik, F., et al. (2011). Epithelial microRNAs regulate gut mucosal immunity via epithelium-T cell crosstalk. *Nat. Immunol.* 12, 239–246.
- Bland, P.W., and Warren, L.G. (1986). Antigen presentation by epithelial cells of the rat small intestine. I. Kinetics, antigen specificity and blocking by anti-la antisera. *Immunology* 58, 1–7.
- Brennecke, P., Anders, S., Kim, J.K., Kołodziejczyk, A.A., Zhang, X., Proserpio, V., Baying, B., Benes, V., Teichmann, S.A., Marioni, J.C., and Heisler, M.G. (2013). Accounting for technical noise in single-cell RNA-seq experiments. *Nat. Methods* 10, 1093–1095.
- Buczacki, S.J., Zecchini, H.I., Nicholson, A.M., Russell, R., Vermeulen, L., Kemp, R., and Winton, D.J. (2013). Intestinal label-retaining cells are secretory precursors expressing Lgr5. *Nature* 495, 65–69.
- Buja, A., and Eyuboglu, N. (1992). Remarks on parallel analysis. *Multivariate Behav. Res.* 27, 509–540.
- Burzyn, D., Kuswanto, W., Kolodkin, D., Shadrach, J.L., Cerletti, M., Jang, Y., Sefik, E., Tan, T.G., Wagers, A.J., Benoist, C., and Mathis, D. (2013). A special population of regulatory T cells potentiates muscle repair. *Cell* 155, 1282–1295.
- Chinen, T., Volchkov, P.Y., Chervonsky, A.V., and Rudensky, A.Y. (2010). A critical role for regulatory T cell-mediated control of inflammation in the absence of commensal microbiota. *J. Exp. Med.* 207, 2323–2330.
- Cordier, A.C., and Haumont, S.M. (1980). Development of thymus, parathyroids, and ultimo-brachial bodies in NMRI and nude mice. *Am. J. Anat.* 157, 227–263.
- Degirmenci, B., Valenta, T., Dimitrieva, S., Hausmann, G., and Basler, K. (2018). GLI1-expressing mesenchymal cells form the essential Wnt-secreting niche for colon stem cells. *Nature* 558, 449–453.
- Denning, T.L., Campbell, N.A., Song, F., Garofalo, R.P., Klimpel, G.R., Reyes, V.E., and Ernst, P.B. (2000). Expression of IL-10 receptors on epithelial cells from the murine small and large intestine. *Int. Immunol.* 12, 133–139.
- el Marjou, F., Janssen, K.P., Chang, B.H., Li, M., Hindie, V., Chan, L., Louvard, D., Champon, P., Metzger, D., and Robine, S. (2004). Tissue-specific and inducible Cre-mediated recombination in the gut epithelium. *Genesis* 39, 186–193.
- Esplugues, E., Huber, S., Gagliani, N., Hauser, A.E., Town, T., Wan, Y.Y., O'Connor, W., Jr., Rongvaux, A., Van Rooijen, N., Haberman, A.M., et al. (2011). Control of TH17 cells occurs in the small intestine. *Nature* 475, 514–518.
- Farin, H.F., Karthaus, W.R., Kujala, P., Rakhsandehroo, M., Schwank, G., Vries, R.G., Kalkhoven, E., Nieuwenhuis, E.E., and Clevers, H. (2014). Paneth cell extrusion and release of antimicrobial products is directly controlled by immune cell-derived IFN- γ . *J. Exp. Med.* 211, 1393–1405.
- Gerbe, F., Sidot, E., Smyth, D.J., Ohmoto, M., Matsumoto, I., Dardalhon, V., Cesses, P., Garnier, L., Pouzolles, M., Brulin, B., et al. (2016). Intestinal epithelial tuft cells initiate type 2 mucosal immunity to helminth parasites. *Nature* 529, 226–230.
- Grün, D., Lyubimova, A., Kester, L., Wiebrands, K., Basak, O., Sasaki, N., Clevers, H., and van Oudenaarden, A. (2015). Single-cell messenger RNA sequencing reveals rare intestinal cell types. *Nature* 525, 251–255.
- Haber, A.L., Biton, M., Rogel, N., Herbst, R.H., Shekhar, K., Smillie, C., Burgin, G., Delorey, T.M., Howitt, M.R., Katz, Y., et al. (2017). A single-cell survey of the small intestinal epithelium. *Nature* 551, 333–339.
- Habib, N., Li, Y., Heidenreich, M., Swiech, L., Avraham-David, I., Trombetta, J.J., Hession, C., Zhang, F., and Regev, A. (2016). Div-Seq: Single-nucleus RNA-Seq reveals dynamics of rare adult newborn neurons. *Science* 353, 925–928.
- Haghverdi, L., Buetner, F., and Theis, F.J. (2015). Diffusion maps for high-dimensional single-cell analysis of differentiation data. *Bioinformatics* 31, 2989–2998.
- Hashimoto, K., Joshi, S.K., and Koni, P.A. (2002). A conditional null allele of the major histocompatibility IA-beta chain gene. *Genesis* 32, 152–153.
- Howie, D., Garcia Rueda, H., Brown, M.H., and Waldmann, H. (2013). Secreted and transmembrane 1A is a novel co-stimulatory ligand. *PLoS ONE* 8, e73610.
- Howitt, M.R., Lavoie, S., Michaud, M., Blum, A.M., Tran, S.V., Weinstock, J.V., Gallini, C.A., Redding, K., Margolskee, R.F., Osborne, L.C., et al. (2016). Tuft cells, taste-chemosensory cells, orchestrate parasite type 2 immunity in the gut. *Science* 351, 1329–1333.
- Iwata, M., Hirakiyama, A., Eshima, Y., Kagechika, H., Kato, C., and Song, S.Y. (2004). Retinoic acid imprints gut-homing specificity on T cells. *Immunity* 21, 527–538.
- Jäger, A., Dardalhon, V., Sobel, R.A., Bettelli, E., and Kuchroo, V.K. (2009). Th1, Th17, and Th9 effector cells induce experimental autoimmune encephalomyelitis with different pathological phenotypes. *J. Immunol.* 183, 7169–7177.
- Johnson, W.E., Li, C., and Rabinovic, A. (2007). Adjusting batch effects in microarray expression data using empirical Bayes methods. *Biostatistics* 8, 118–127.
- Kaiserlian, D., Vidal, K., and Revillard, J.P. (1989). Murine enterocytes can present soluble antigen to specific class II-restricted CD4+ T cells. *Eur. J. Immunol.* 19, 1513–1516.
- Kim, J.M., Rasmussen, J.P., and Rudensky, A.Y. (2007). Regulatory T cells prevent catastrophic autoimmunity throughout the lifespan of mice. *Nat. Immunol.* 8, 191–197.
- Kowalczyk, M.S., Tirosh, I., Heckl, D., Rao, T.N., Dixit, A., Haas, B.J., Schneider, R.K., Wagers, A.J., Ebert, B.L., and Regev, A. (2015). Single-cell RNA-seq reveals changes in cell cycle and differentiation programs upon aging of hematopoietic stem cells. *Genome Res.* 25, 1860–1872.
- Langmead, B., Trapnell, C., Pop, M., and Salzberg, S.L. (2009). Ultrafast and memory-efficient alignment of short DNA sequences to the human genome. *Genome Biol.* 10, R25.
- Li, B., and Dewey, C.N. (2011). RSEM: accurate transcript quantification from RNA-Seq data with or without a reference genome. *BMC Bioinformatics* 12, 323.
- Lindemans, C.A., Calafiore, M., Mertelsmann, A.M., O'Connor, M.H., Dudakov, J.A., Jenq, R.R., Velardi, E., Young, L.F., Smith, O.M., Lawrence, G., et al. (2015). Interleukin-22 promotes intestinal-stem-cell-mediated epithelial regeneration. *Nature* 528, 560–564.
- Mabbott, N.A., Donaldson, D.S., Ohno, H., Williams, I.R., and Mahajan, A. (2013). Microfold (M) cells: important immunosurveillance posts in the intestinal epithelium. *Mucosal Immunol.* 6, 666–677.
- Macosko, E.Z., Basu, A., Satija, R., Nemesh, J., Shekhar, K., Goldman, M., Tirsh, I., Bialas, A.R., Kamitaki, N., Martersteck, E.M., et al. (2015). Highly parallel genome-wide expression profiling of individual cells using nanoliter droplets. *Cell* 161, 1202–1214.
- Madison, B.B., Dunbar, L., Qiao, X.T., Braunstein, K., Braunstein, E., and Guzmán, D.L. (2002). Cis elements of the villin gene control expression in restricted domains of the vertical (crypt) and horizontal (duodenum, cecum) axes of the intestine. *J. Biol. Chem.* 277, 33275–33283.
- Madsen, L., Labrecque, N., Engberg, J., Dierich, A., Svejgaard, A., Benoist, C., Mathis, D., and Fugger, L. (1999). Mice lacking all conventional MHC class II genes. *Proc. Natl. Acad. Sci. USA* 96, 10338–10343.
- Mombaerts, P., Clarke, A.R., Rudnicki, M.A., Iacomini, J., Itohara, S., Lafaille, J.J., Wang, L., Ichikawa, Y., Jaenisch, R., Hooper, M.L., et al. (1992). Mutations in T-cell antigen receptor genes alpha and beta block thymocyte development at different stages. *Nature* 360, 225–231.
- Muñoz, J., Stange, D.E., Schepers, A.G., van de Wetering, M., Koo, B.-K., Itzkovitz, S., Volckmann, R., Kung, K.S., Koster, J., Radulescu, S., et al. (2012). The Lgr5 intestinal stem cell signature: robust expression of proposed quiescent '+4' cell markers. *EMBO J.* 31, 3079–3091.
- Nusse, Y.M., Savage, A.K., Marangoni, P., Rosendahl-Huber, A.K.M., Landman, T.A., de Sauvage, F.J., Locksley, R.M., and Klein, O.D. (2018). Parasitic helminths induce fetal-like reversion in the intestinal stem cell niche. *Nature* 559, 109–113.

- Picelli, S., Faridani, O.R., Bjorklund, A.K., Winberg, G., Sagasser, S., and Sandberg, R. (2014). Full-length RNA-seq from single cells using Smart-seq2. *Nat. Protoc.* 9, 171–181.
- Ramilowski, J.A., Goldberg, T., Harshbarger, J., Kloppmann, E., Lizio, M., Satagopam, V.P., Itoh, M., Kawaji, H., Carninci, P., Rost, B., and Forrest, A.R. (2015). A draft network of ligand-receptor-mediated multicellular signalling in human. *Nat. Commun.* 6, 7866.
- Rosvall, M., and Bergstrom, C.T. (2008). Maps of random walks on complex networks reveal community structure. *Proc. Natl. Acad. Sci. USA* 105, 1118–1123.
- Rubin, D.B. (1981). The Bayesian bootstrap. *Ann. Stat.* 9, 130–134.
- Saha, S., Aranda, E., Hayakawa, Y., Bhanja, P., Atay, S., Brodin, N.P., Li, J., Asfaha, S., Liu, L., Tailor, Y., et al. (2016). Macrophage-derived extracellular vesicle-packaged WNTs rescue intestinal stem cells and enhance survival after radiation injury. *Nat. Commun.* 7, 13096.
- Sato, T., Vries, R.G., Snippert, H.J., van de Wetering, M., Barker, N., Stange, D.E., van Es, J.H., Abo, A., Kujala, P., Peters, P.J., and Clevers, H. (2009). Single Lgr5 stem cells build crypt-villus structures in vitro without a mesenchymal niche. *Nature* 459, 262–265.
- Sato, T., van Es, J.H., Snippert, H.J., Stange, D.E., Vries, R.G., van den Born, M., Barker, N., Shroyer, N.F., van de Wetering, M., and Clevers, H. (2011). Paneth cells constitute the niche for Lgr5 stem cells in intestinal crypts. *Nature* 469, 415–418.
- Schneider, C.A., Rasband, W.S., and Eliceiri, K.W. (2012). NIH Image to ImageJ: 25 years of image analysis. *Nat. Methods* 9, 671–675.
- Shalek, A.K., Satija, R., Shuga, J., Trombetta, J.J., Gennert, D., Lu, D., Chen, P., Gertner, R.S., Gaublomme, J.T., Yosef, N., et al. (2014). Single-cell RNA-seq reveals dynamic paracrine control of cellular variation. *Nature* 510, 363–369.
- Shi, H.N., Koski, K.G., Stevenson, M.M., and Scott, M.E. (1997). Zinc deficiency and energy restriction modify immune responses in mice during both primary and challenge infection with *Heligmosomoides polygyrus* (Nematoda). *Parasite Immunol.* 19, 363–373.
- Shoshkes-Carmel, M., Wang, Y.J., Wangensteen, K.J., Tóth, B., Kondo, A., Massasa, E.E., Itzkovitz, S., and Kaestner, K.H. (2018). Subepithelial telocytes are an important source of Wnts that supports intestinal crypts. *Nature* 557, 242–246.
- Stappenbeck, T.S., and Miyoshi, H. (2009). The role of stromal stem cells in tissue regeneration and wound repair. *Science* 324, 1666–1669.
- Tanoue, T., Atarashi, K., and Honda, K. (2016). Development and maintenance of intestinal regulatory T cells. *Nat. Rev. Immunol.* 16, 295–309.
- Tetteh, P.W., Basak, O., Farin, H.F., Wiebrands, K., Kretzschmar, K., Begthel, H., van den Born, M., Korving, J., de Sauvage, F., van Es, J.H., et al. (2016). Replacement of lost Lgr5-positive stem cells through plasticity of their enterocyte-lineage daughters. *Cell Stem Cell* 18, 203–213.
- Thelemann, C., Eren, R.O., Coutaz, M., Brasseit, J., Bouzourene, H., Rosa, M., Duval, A., Lavanchy, C., Mack, V., Mueller, C., et al. (2014). Interferon- γ induces expression of MHC class II on intestinal epithelial cells and protects mice from colitis. *PLoS ONE* 9, e86844.
- Tirosh, I., Izar, B., Prakadan, S.M., Wadsworth, M.H., 2nd, Treacy, D., Trombetta, J.J., Rotem, A., Rodman, C., Lian, C., Murphy, G., et al. (2016). Dissecting the multicellular ecosystem of metastatic melanoma by single-cell RNA-seq. *Science* 352, 189–196.
- van der Flier, L.G., and Clevers, H. (2009). Stem cells, self-renewal, and differentiation in the intestinal epithelium. *Annu. Rev. Physiol.* 71, 241–260.
- van der Maaten, L. (2014). Accelerating t-SNE using Tree-Based Algorithms. *J. Mach. Learn. Res.* 15, 3221–3245.
- von Moltke, J., Ji, M., Liang, H.E., and Locksley, R.M. (2016). Tuft-cell-derived IL-25 regulates an intestinal ILC2-epithelial response circuit. *Nature* 529, 221–225.
- Wang, T., Huang, C., Lopez-Coral, A., Slentz-Kesler, K.A., Xiao, M., Wherry, E.J., and Kaufman, R.E. (2012). K12/SECTM1, an interferon- γ regulated molecule, synergizes with CD28 to costimulate human T cell proliferation. *J. Leukoc. Biol.* 91, 449–459.
- Yan, K.S., Janda, C.Y., Chang, J., Zheng, G.X.Y., Larkin, K.A., Luca, V.C., Chia, L.A., Mah, A.T., Han, A., Terry, J.M., et al. (2017). Non-equivalence of Wnt and R-spondin ligands during Lgr5 $^{+}$ intestinal stem-cell self-renewal. *Nature* 545, 238–242.
- Young, M.D., Wakefield, M.J., Smyth, G.K., and Oshlack, A. (2010). Gene ontology analysis for RNA-seq: accounting for selection bias. *Genome Biol.* 11, R14.
- Ziegler, S.F., and Artis, D. (2010). Sensing the outside world: TSLP regulates barrier immunity. *Nat. Immunol.* 11, 289–293.

STAR★METHODS

KEY RESOURCES TABLE

REAGENT or RESOURCE	SOURCE	IDENTIFIER
Antibodies		
rabbit anti-DCLK1	Abcam	Cat#ab37994; RRID: AB_873538
mouse anti-E-cadherin	BD Biosciences	Cat#610181; RRID:AB_397580
rat anti-CD4	BioLegend	Cat#100402; RRID:AB_312687
rabbit anti-CD4	Abcam	Cat#ab183685; RRID:AB_2686917
rat anti-Lysozyme	Dako	Cat#A0099; RRID:AB_2341230
rabbit anti-GFP	Cell Signaling Technologies	Cat#2956S; RRID:AB_1196615
anti-mouse I-A/I-E	BioLegend	Cat#107601; RRID:AB_313316
Goat anti-Mouse IgG (H+L) Cross-Adsorbed Secondary Antibody, Alexa Fluor 405	Thermo Fisher Scientific	Cat#A-31553, RRID:AB_221604
Goat anti-Mouse IgG (H+L) Cross-Adsorbed Secondary Antibody, Alexa Fluor 488	Thermo Fisher Scientific	Cat#R37120, RRID:AB_2556548
Goat anti-Mouse IgG (H+L) Cross-Adsorbed Secondary Antibody, Alexa Fluor 647	Thermo Fisher Scientific	Cat#A28181, RRID:AB_2536165
Goat anti-Rat IgG (H+L) Cross-Adsorbed Secondary Antibody, Alexa Fluor 488	Thermo Fisher Scientific	Cat#A-11006, RRID:AB_2534074
Goat anti-Rat IgG (H+L) Cross-Adsorbed Secondary Antibody, Alexa Fluor 594	Thermo Fisher Scientific	Cat#SA5-10020, RRID:AB_2556600
Goat anti-Rabbit IgG (H+L) Cross-Adsorbed Secondary Antibody, Alexa Fluor 488	Thermo Fisher Scientific	Cat#A-11008, RRID:AB_143165
Goat anti-Rabbit IgG (H+L) Cross-Adsorbed Secondary Antibody, Alexa Fluor 594	Thermo Fisher Scientific	Cat#A-11012, RRID:AB_2534079
EpCAM	Thermo Fisher Scientific	Cat#47-5791-82; RRID: AB_2573986
CD45 PE	Thermo Fisher Scientific	Cat#12-0451-81; RRID:AB_465667
CD45 FITC	BioLegend	Cat#103121; RRID:AB_493532
Ter119	Thermo Fisher Scientific	Cat#12-5921-81; RRID:AB_466041
CD31	Thermo Fisher Scientific	Cat#12-0311-81; RRID:AB_465631
CD44	BioLegend	Cat#103008; RRID:AB_312959
CD25	BioLegend	Cat#102016; RRID:AB_312865
CD62L	BioLegend	Cat#104412; RRID:AB_313099
CD4 FITC	Thermo Fisher Scientific	Cat#11-0041-81; RRID:AB_464891
CD4 APC/Cy7	BioLegend	Cat#100526; RRID:AB_312727
MHC Class II (I-A/I-E) FITC	Thermo Fisher Scientific	Cat#11-5321-81; RRID:AB_465231
MHC Class II (I-A/I-E) PE	BioLegend	Cat#107607, RRID:AB_313322
anti-mouse MHC Class II (I-A/I-E)	Bio X Cell	Cat#BE0108, RRID:AB_10949298
IgG2b	Bio X Cell	Cat#BE0090, RRID:AB_1107780
Mm-Lgr5-C1	ACDBio	Cat#312171
Mm-Trpm5-C2	ACDBio	Cat#525101-C2
Mm-Defa23-C3	ACDBio	Custom probe
Mm-OLFM4-C2	ACDBio	Cat#311831
Mm-H2-Ab1-C2	ACDBio	Cat#414731-C2
Mm-Ki67-C3	ACDBio	Cat#591771-C3
Mm-Lgr5-C2	ACDBio	Cat#312171-C2
Mm-Ki67-C1	ACDBio	Cat#591771
Mm-Cyp2e1-C2	ACDBio	Cat#402781-C2

(Continued on next page)

Continued

REAGENT or RESOURCE	SOURCE	IDENTIFIER
Mm-Psrc1-C1	ACDBio	Cat#466889
Mm-Itgax-C3	ACDBio	Cat#311508-C3
Bacterial and Virus Strains		
<i>S. Typhimurium</i>	Massachusetts General Hospital (Shi Lab)	SL1344
Chemicals, Peptides, and Recombinant Proteins		
OVA (323 - 339)	Ana-Spec	Cat#AS-27024
DQ Ovalbumin	Thermo Fisher Scientific	Cat#D12053
Matrigel	Corning	Cat#356231
Jagged-1	Ana-Spec	Cat#AS-61298
Recombinant Murine EGF	PrepoTech	Cat#315-09
R-Spondin-1	R&D Systems	Cat#3474-RS-050
Recombinant Murine Noggin	PrepoTech	Cat#250-38
Y-276432 dihydrochloride monohydrate	Tocris	Cat#1254
N-acetyl-1-cysteine	Sigma-Aldrich	Cat#A9165-5G
N-2 Supplement	Thermo Fisher Scientific	Cat#17502048
B-27 Supplement	Thermo Fisher Scientific	Cat#12587-010
Wnt-3a Protein	R&D Systems	Cat#5036-WN-010
Recombinant Murine IFN γ	PrepoTech	Cat#315-05
Recombinant Murine IL-13	PrepoTech	Cat#210-13A
Recombinant Murine IL-17A	PrepoTech	Cat#210-17
Recombinant Murine IL-10	PrepoTech	Cat#210-10
Diphtheria Toxin	Sigma-Aldrich	Cat#D05564
Tamoxifen	Sigma-Aldrich	Cat#T5648
Critical Commercial Assays		
Nextera XT Sample Preparation Kit	Illumina	Cat#FC-131-1096
Naive CD4+ T Cell Isolation Kit	Miltenyi Biotec	Cat#130-104-453
10X Chromium Single Cell 3' Kit	10X Genomics	Cat#120237
Mouse IL-2 Flex Set	BD Bioscience	Cat#558297
CellTrace Violet Proliferation Kit	Thermo Fisher Scientific	Cat#C34557
RNAscope Multiplex Fluorescent Detection Kit v2	ACDBio	Cat#323110
Deposited Data		
Single cell mRNA-seq data	This paper	GEO: GSE106510
Mendeley	This paper	https://data.mendeley.com/datasets/9rvb5p2ydh/edit
Experimental Models: Organisms/Strains		
Mouse: C57BL/6J	Jackson Laboratory	Cat#000664 RRID:IMSR_JAX:000664
Mouse: MHCII-KO	Jackson Laboratory	Cat#003584 RRID:IMSR_JAX:003584
Mouse: Lgr5-EGFP-IRES-CreER ^{T2}	Jackson Laboratory	Cat#008875 RRID:IMSR_JAX:008875
Mouse: Foxp3 ^{DTR}	Jackson Laboratory	Cat#016958 RRID:IMSR_JAX:016958
Mouse: B6 Nude	Jackson Laboratory	Cat#000819 RRID:IMSR_JAX:000819
Mouse: TCR β KO	Jackson Laboratory	Cat#002118 RRID:IMSR_JAX:002118

(Continued on next page)

Continued

REAGENT or RESOURCE	SOURCE	IDENTIFIER
Mouse: B6.Cg-Tg(TcraTcrb)425Cbn/J (OTII mice)	Jackson Laboratory	Cat#004194 RRID:IMSR_JAX:004194
Mouse: Villin-Cre	Jackson Laboratory	Cat#004586 RRID:IMSR_JAX:004586
Mouse: Villin-CreER ^{T2}	el Marjou et al., 2004	N/A
Mouse: MHCII ^{f/f} (B6.129X1-H2-Ab1 ^{tm1Koni} /J)	Jackson Laboratory	Cat#013181 RRID:IMSR_JAX: 013181
Mouse: MHCII ^{gut-/-} (MHCII ^{f/f} + Villin-Cre)	This Paper	N/A
Mouse: MHCII ^{Δgut} (MHCII ^{f/f} + Villin-CreER ^{T2})	This Paper	N/A
Mouse: MHCII ^{ΔISC} (MHCII ^{f/f} + Lgr5-EGFP-IRES-CreER ^{T2})	This Paper	N/A
<i>H. polygyrus</i>	Massachusetts General Hospital (Shi Lab)	N/A
Oligonucleotides		
Reverse Transcription DNA oligonucleotide primer (RNase-free, 100 μM)	IDT	5'-AAGCAGTGGTATCAACGCAGAGTACT(30)VN-3'
SMARTER TSO (with LNA)	Exiqon	5'-AAGCAGTGGTATCAACGCAGAGTCrGrG+G-3'
PCR oligonucleotide primer	IDT	5'-AAGCAGTGGTATCAACGCAGAGT-3'
Software and Algorithms		
ImageJ	Schneider et al., 2012	https://imagej.nih.gov/ij/
GraphPad Prism	GraphPad Software	https://www.graphpad.com/scientific-software/prism/
FlowJo	TreeStar	https://www.flowjo.com/solutions/flowjo
Bowtie	Langmead et al., 2009	http://bowtie-bio.sourceforge.net/index.shtml
10x cellranger	10X Genomics	https://support.10xgenomics.com/single-cell/software/overview/welcome
RSEM	Li and Dewey, 2011	http://deweylab.github.io/RSEM/
Python code for mRNA quantification from smFISH images	This paper	https://github.com/adamh-broad/image_analysis/
R code for single-cell RNA-seq analysis	Haber et al., 2017	https://github.com/adamh-broad/single_cell_intestine

CONTACT FOR REAGENT AND RESOURCE SHARING

Further information and requests for resources and reagents should be directed to and will be fulfilled by the Lead Contact Ramnik J. Xavier (xavier@molbio.mgh.harvard.edu).

EXPERIMENTAL MODEL AND SUBJECT DETAILS**Mice**

All mouse work was performed in accordance with the Institutional Animal Care and Use Committees (IACUC) and relevant guidelines at the Broad Institute and MIT, with protocols 0055-05-15 and 0612-058-15, respectively. C57BL/6J WT, Lgr5-EGFP-IRES-CreER^{T2} (Lgr5-GFP), MHCII-KO, Foxp3-DTR, B6 Nude, TCRβ-KO mice, and B6.Cg-Tg(TcraTcrb)425Cbn/J (OTII) were obtained from the Jackson Laboratory (Bar Harbor, ME). MHCII^{gut-/-}, MHCII^{Δgut} and MHCII^{ΔISC} mice were generated by crossing H2-Ab1^{f/f} (Jackson laboratory) with Villin-Cre, Villin-CreER^{T2} or Lgr5-EGFP-IRES-CreER^{T2}, respectively. Both male and female age-matched mice from 7 to 14 weeks of age were used for all experiments in this study. Littermates of the same genotype, sex, and age were randomly assigned to experimental groups. All mice were housed under specific-pathogen-free (SPF) conditions at the Broad Institute or MIT animal facilities; infection experiments were conducted at the laboratory of Dr. HN Shi, maintained under specific pathogen-free conditions at Massachusetts General Hospital (Charlestown, MA), with protocol 2003N000158.

Infection models

S. enterica infection, mice were infected with a naturally streptomycin-resistant SL1344 strain of *S. Typhimurium* (10⁸ cells).

H. polygyrus was propagated as previously described (Shi et al., 1997). Third-stage larvae (L3) of *H. polygyrus* were obtained by culturing the feces of infected stock CO1 mice on moist filter paper for seven days. Mice were intubated with 200L, in 20/LI of de-ionized water. The accuracy of the dose was estimated by direct counts of the numbers of larvae in five sham doses, which were dispensed into plastic Petri dishes before the experimental infection. At necropsy, the intestine was open longitudinally, and worms were removed for quantification under a binocular microscope (counting only worm tails).

In vitro and ex vivo cultures

Naive OTII cells were isolated from the spleen of 7-10 weeks old OTII female mice.

Th cell polarization *in vitro*. CD4⁺ naive (CD44^{low}CD62L⁺CD25⁻) T cells were isolated from spleen and lymph nodes of 7–10 weeks old C57BL/6J mice using flow cytometry cell sorting. The purity of isolated T cell populations routinely exceeded 98%. Naive T cells were stimulated with plate-bound anti-CD3 (145-2C11, 1mg/ml) and anti-CD28 (PV-1, 1mg/ml) and polarizing cytokines (Th1: 4 ng/ml IL-12; Th2: 4 ng/ml IL-4; Th17: 10 ng/ml IL-6, 2 ng/ml TGF-β1; iT_{reg}: 5 ng/ml TGF-β1; all cytokines from R&D) (Jäger et al., 2009).

METHOD DETAILS

BrdU and EDU incorporation

EdU or BrdU was injected intraperitoneally (IP) into Lgr5-GFP mice at 100 mg kg⁻¹ for 2 or 4 hr before tissue collection.

MHCII deletion in intestinal cells

Cre activity was induced in 7-10 weeks old H2-Ab1 floxed mice that express or not expressing Cre by intraperitoneal injection (IP) of tamoxifen (Sigma-Aldrich), diluted in corn oil, 4 mg per injection, 3 or 5 times, every other day. Mice were sacrificed 10 or 15 days after the first injection. For *H. polygyrus* infection following MHCII ablation, we induced deletion of MHCII^{ΔISC} by 3 injections every other day for 6 days in total prior to infection.

S. enterica and *H. polygyrus* infection

C57BL/6J, MHCII^{gut-/-} or MHCII^{ΔISC} and their control littermates (MHCII^{f/f}) mice were infected with 200 third-stage larvae of *H. polygyrus*. MHCII^{ΔISC} and their control siblings (MHCII^{f/f}) were induced with 4 mg/injection of Tamoxifen for 6 days prior to *H. polygyrus* infection. Mice were sacrificed 3, 4, 10 days or 6 weeks following *H. polygyrus* infection. For the MHCII blocking experiment, C57BL/6J mice infected with *H. polygyrus* were injected with 500 µg of blocking anti-mouse MHCII antibody (BioXCell) or Rat IgG2b isotype control (BioXCell) one-day prior to and for 2 consecutive days after *H. polygyrus* infection. For *S. enterica* infection, C57BL/6J mice were infected with a naturally streptomycin-resistant SL1344 strain of *S. Typhimurium* (10⁸ cells) and were sacrificed 48 hr after infection.

Diphtheria toxin

Foxp3-DTR and WT C57BL/6J mice were injected intraperitoneally with diphtheria toxin (DT) at 22.5ng/g body weight every other day for either 4 or 7 days and then sacrificed for tissue collection.

Epithelial cell dissociation and crypt isolation

For all mice, crypts were isolated from the whole small intestine or the duodenum, jejunum, and ileum compartments to account for regional distribution of Lgr5⁺ ISCs. The small intestine was extracted and rinsed in cold PBS. The tissue was opened longitudinally and sliced into small fragments roughly 0.2 cm long. The tissue was incubated in 20mM EDTA-PBS on ice for 90 min, while shaking every 30 min. The tissue was then shaken vigorously and the supernatant was collected as fraction 1 in a new conical tube. The tissue was incubated in fresh EDTA-PBS and a new fraction was collected every 30 min. Fractions were collected until the supernatant consisted almost entirely of crypts. The final fraction (enriched for crypts) was filtered through a 70µm filter, washed twice in PBS, centrifuged at 300 g for 3 min, and dissociated with TrypLE Express (Invitrogen) for 1 min at 37°C. The single-cell suspension was then passed through a 40 µm filter and stained for fluorescence- activated cell sorting (FACS) machine (Astrios) sorting for either scRNA-seq method (below).

Immune cell isolation

Immune cells from the Lamina Propria were isolated enzymatically by incubating the small intestine with Liberase TM (100 µg/mL, Sigma) and DNasel (10 µg/mL, Sigma) for 30 min at 37°C. Immune cells were also isolated from the mesenteric lymph nodes (mLN). Cells were then incubated with CD3, CD4, CD45, TCRβ, CD11c, I-A/I-E, IL17a, IFNγ or IL13 FACS-labeled antibodies and either used for analysis or sorted for scRNA-seq.

Naive OTII cells were isolated from the spleen of 7-10 week old OTII mice. Cells were purified using the Naive CD4+ T Cell Isolation Kit (Miltenyi Biotec, 130-104-453) per manufacturer's recommendations. Cells were then FACS sorted for CD25⁻CD4⁺CD44^{low}CD62L⁺ to obtain 99% purity of naive OTII cells.

Intestinal organoid cultures

Following crypt isolation from the whole small intestine of both male and female mice, the single-cell suspension was re-suspended in Matrigel (BD Bioscience) with 1 μ M Jagged-1 peptide (Ana-Spec). Roughly 300 crypts embedded in 25 μ L of Matrigel were seeded onto each well of a 24-well plate. Once solidified, the Matrigel was incubated in 600 μ L culture medium (Advanced DMEM/F12, Invitrogen) with streptomycin/penicillin and glutamax and supplemented with EGF (100 ng/mL, Peprotech), R-Spondin-1 (600ng/mL, R&D), Noggin (100ng/mL, Preptech), Y-276432 dihydrochloride monohydrate (10 μ M, Tochris), N-acetyl-1-cysteine (1 μ M, Sigma-Aldrich), N2 (1X, Life Technologies), B27 (1X, Life Technologies) and Wnt3A (25ng/mL, R&D Systems). Fresh media was replaced on day 3, and organoids were passaged by dissociation with TrypLE and re-suspended in new Matrigel on day 6 with a 1:3 split ratio.

T helper cell co-culture experiments

Organoids were cultured with Th1, Th2, Th17 or iT_{regs}. Roughly 10,000 T helper cells were added to each well of 500 organoids and were supplemented either to the medium or suspended in the Matrigel. Treated organoids were dissociated and subjected to droplet based scRNA-seq.

Cytokine treated organoids

Organoids were additionally treated with 0.5u/ml IFN γ , 20 ng/ml IL-13, 20 ng/ml IL-17A or 10ng/ml IL-10 in the culture medium for 3 days.

Re-seeding after cytokine treatment

500 organoids/well were treated with cytokines, as in the cytokine treated organoids above, collected after 3 days and then re-seeded at 500 organoids/well in fresh media without cytokines. Each day, images were taken at 2X magnification and quantification of organoids number was performed with the ImageJ software.

Antigen processing and presentation

Processing

3 \times 10⁴ sort-purified CD11c $^+$ DCs from the spleen or EpCAM $^+$ cells isolated from the small intestine were cultured with 10 μ g/ml DQ Ovalbumin (Thermo Fisher Scientific) at 4°C, 37°C or with no DQ Ovalbumin for 2 hr, washed and analyzed via flow cytometry. Additionally, EpCAM $^+$ DQ $^+$ cells were FACS sorted individually into 96 well plates with TCL and 1% 2-mercaptoethanol and then processed via plate-based scRNA-seq (as described below).

Presentation

5x10³ sort-purified Lgr5 high EpCAM $^+$, 5x10³ sort-purified Lgr5 negative EpCAM $^+$ or 2.5x10³ CD11c $^+$ DCs were cultured with 5x10⁴ naive OTII cells in the organoid culture medium above (without Matrigel), with or without 15 μ g/ml Ovalbumin peptide (Anaspec, OVA323-339) at 37°C for 72 hr. T cell activation was measured through IL-2 levels in the supernatant using the BD Cytometric Bead Array Mouse IL-2 Flex Set (BD Bioscience) per manufacturer's directions. Capture bead solution was added to the supernatant, followed by the detection bead solution, a wash, and then resuspended in FACS buffer to be analyzed via flow cytometry. T cell proliferation was assessed using the CellTrace Violet Proliferation Kit (Thermo Fisher Scientific) per manufacturer's instructions. Prior to seeding, naive OTII cells were incubated for 20 min with the CellTrace solution in PBS and then washed in 1X PBS with 1% BSA. Following co-culture, OTII cells were washed with PBS, stained for CD4 and assessed via flow cytometry.

Cell sorting

For plate-based, full-length scRNA-seq, FACS (Astrios) was used to sort one single cell into each well of a 96-well PCR plate containing 5 μ L of TCL buffer with 1% 2- mercaptoethanol. The cells were stained for 7AAD $^-$ (Life Technologies), CD45 $^-$ (eBioscience), CD31 $^-$ (eBioscience), Ter119 $^-$ (eBioscience), EpCAM $^+$ (eBioscience), and for specific epithelial cells were also stained for CD24 $^{+/-}$ (eBioscience) and c-Kit $^{+/-}$ (eBioscience). To enrich for specific IEC populations, cells were isolated from Lgr5-GFP mice, stained with the antibodies mentioned above and gated for GFP-high (stem cells), GFP-low (TAs), GFP $^-$ /CD24 $^{+/-}$ /c-Kit $^{+/-}$ (secretory lineages) or EpCAM $^+$ (epithelial cells). A population control of 200 cells was sorted into one well and a no-cell control was sorted into another well. After sorting, the plate was sealed tightly with a Microseal F and centrifuged at 800 g for 1 min. The plate was immediately frozen on dry ice and kept at -80°C until ready for the lysate cleanup. Bulk population cells were sorted into an Eppendorf tube containing 100 μ L solution of TCL with 1% 2-mercaptoethanol and stored at -80°C.

For droplet-based scRNA-seq, cells were sorted with the same parameters as described for plate-based scRNA-seq, but into an Eppendorf tube containing 50 μ L of 1X PBS with 0.4% BSA and stored on ice until proceeding to the GemCode Single Cell Platform or the Chromium Single Cell 3' Library.

Plate-based scRNA-seq

Libraries were prepared using a modified SMART-Seq2 protocol as previously reported (Picelli et al., 2014). RNA lysate cleanup was performed using RNAClean XP beads (Agencourt), followed by reverse transcription with Maxima Reverse Transcriptase (Life Technologies) and whole transcription amplification (WTA) with KAPA HotStart HIFI 2 \times ReadyMix (Kapa Biosystems) for 21 cycles. WTA products were purified with Ampure XP beads (Beckman Coulter), quantified with Qubit dsDNA HS Assay Kit (ThermoFisher), and assessed with a high sensitivity DNA chip (Agilent). RNA-seq libraries were constructed from purified WTA products using Nextera XT DNA Library Preparation Kit (Illumina). On each plate, the population and no-cell controls were processed using the same method as the single cells. The libraries were sequenced on an Illumina NextSeq 500.

Droplet-based scRNA-seq

Single cells were processed through the GemCode Single Cell Platform per manufacturer's recommendations using the GemCode Gel Bead, Chip and Library Kits (V1) or single cell suspensions were loaded onto 3' library chips as per the manufacturer's protocol for the Chromium Single Cell 3' Library (V2) (10X Genomics; PN-120233). Briefly, single cells were partitioned into Gel Beads in Emulsion (GEMs) in the GemCode/Chromium instrument with cell lysis and barcoded reverse transcription of RNA, followed by amplification, shearing and 5' adaptor and sample index attachment. An input of 6,000 single cells was added to each channel with a recovery rate of roughly 1,500 cells. Libraries were sequenced on an Illumina Nextseq 500.

Div-Seq

Lgr5-GFP mice were intraperitoneally (IP) injected with 100 mg kg⁻¹ EdU from Click-iT Plus EdU Pacific Blue Flow Cytometry Assay Kit (Thermo Fisher Scientific) for 2 hr and then sacrificed. Crypts were isolated as described above and Lgr5⁺ cells were FACS sorted into PBS, spun down to remove the supernatant, flash frozen and stored in -80°C. Nuclei were isolated using EZ Prep NUC-101 (Sigma) per manufacturer's recommendation, and then incubated in the Click-iT Cocktail per manufacturer's recommendations for 30 min, washed in 1X PBS with 1% BSA and counterstained with Vybrant DyeCycle Ruby stain (Thermo Fisher Scientific) for 15 min. Nuclei were then individually sorted into the wells of 96 well plates with TCL+1% 2-mercaptoethanol as previously described (Habib et al., 2016) using FACS, based on positive Ruby and either EdU^{high} or EdU^{low}.

Plate-based single-nucleus RNA-seq (snRNA-Seq) was then performed as described above for scRNA-seq.

Immunofluorescence and single-molecule fluorescence *in situ* hybridization (smFISH)

Immunofluorescence (IFA) and immunohistochemistry (IHC)

Staining of small intestinal tissue was conducted as previously described (Biton et al., 2011). Tissues were fixed for 14 hr in formalin, embedded in paraffin and cut into 5 µm thick sections. Sections were deparaffinized with standard techniques, incubated with primary antibodies overnight at 4°C, and then incubated with secondary antibodies at room temperature for 30 min. Slides were mounted with Slowfade Mountant+DAPI (Life Technologies, S36964) and sealed for IFA, or treated with hematoxylin, dehydrated and mounted for IHC.

Single-molecule fluorescence *in situ* hybridization (smFISH)

RNAscope Fluorescent Multiplex and RNAscope Multiplex Fluorescent v2 (Advanced Cell Diagnostics) were used per manufacturer's recommendations with the following alterations. Target Retrieval boiling time was adjusted to 12 min and incubation with Protease IV at 40°C was adjusted to 8 min. Slides were mounted with Slowfade Mountant+DAPI (Life Technologies, S36964) and sealed.

Combined IFA and smFISH was implemented by first performing smFISH, as described above, with the following alterations. After Amp 4, tissue sections were washed in washing buffer, incubated with primary antibodies overnight at 4°C, washed in 1x TBST 3 times and then incubated with secondary antibodies for 30 min at room temperature. Slides were mounted with Slowfade Mountant+DAPI (Life Technologies, S36964) and sealed.

Image analysis

Images of tissue sections were taken with a confocal microscope Fluorview FV1200 using Kalman and sequential laser emission to reduce noise and signal overlap. Scale bars were added to each image using the confocal software FV10-ASW 3.1 Viewer. Images were overlaid and visualized using ImageJ software (Schneider et al., 2012).

Two-photon intra-vital microscopy (2P-IVM) of T cells and Lgr5⁺ ISCs

To generate gut-homing T cells visualized by 2P-IVM, a combination of modified protocols (Esplugues et al., 2011; Iwata et al., 2004) was used. CD4⁺ T cells were isolated from spleen, PLN and mLN from β-actin-RFP mice using a MACS CD4 T cell positive-selection kit (Miltenyi clone L3T4) following the manufacturer's instructions. Plates were pre-treated with 5 µg/mL anti-CD3 (clone 145-2C11) and 1 µg/mL anti-CD28 (clone 37.51) and 1 × 10⁶ CD4⁺ T cells were added to each well for a final volume of 2.5mL in complete RPMI1640 media supplemented with all-trans Retinoic Acid (100nM, Sigma R2625). The T cells were cultured for 96 hr before replacing half of the volume with fresh media containing 20U/mL of rIL-2 and then cultured for another 48 hr. Before adoptive transfer into Lgr5-GFP hosts, the gut-homing phenotype was validated with flow cytometry for α4β7 and CCR9 expression. 1 × 10⁷ cells were then transferred into recipient mice for 2 hr, and treated with 20ug of anti-CD3 (clone 2C11). 2P-IVM was performed 72 hr following transfer. The small intestine was surgically exposed through a laparotomy incision. Anesthetized mice were placed on a custom-built stage with a loop of the intact small intestine fixed to a temperature-controlled metallic support to facilitate exposure of the serosal aspect to a water-immersion 20X objective (0.95 numerical aperture) of an upright microscope (Prairie Technologies). A Mai Tai Ti:sapphire laser (Spectra-Physics) was tuned between 870nm and 900nm for multiphoton excitation and second-harmonic generation. For dynamic analysis of cell interaction in four dimensions, several X/Y sections (512x512) with Z spacing ranging from 2 µm to 4 µm were acquired every 15-20 s with an electronic zoom varying from 1X to 3X. Emitted light and second-harmonic signals were directed through 450/80-nm, 525/50-nm and 630/120-nm band-pass filters and detected with non-descanned detectors. Post-acquisition image analysis, volume-rendering and four-dimensional time-lapse videos were performed using Imaris software (Bitplane scientific software).

QUANTIFICATION AND STATISTICAL ANALYSIS

Image quantification

Quantification of proliferating stem cells

Combined IFA and smFISH images of WT C57BL/6J small intestinal tissues were assessed by staining for E-Cadherin to mark cell borders, the canonical proliferation marker *mKi67*, and either the common ISC marker *Lgr5*, our predicted IcISC markers (*Cyp2e1* or *Fgf4*) or our predicted hcISC markers (*Psrc1* or *Cenpf*). A line was drawn to establish the bottom of the crypt, termed “stem cell zone,” and quantification was only assessed within that zone. For each ISC subset marker, more than 10 randomly chosen intact crypts were analyzed. Cells were examined by double blind quantification and were determined double positive if they co-expressed *mKi67* and one of the ISC subset markers. Proliferating cells in each ISC subset was measured by calculating the fraction of double positive cells out of all cells positive for the specific ISC subset marker.

Automated quantification of *Lgr5* mRNA molecules in smFISH images of intestinal crypts within different mouse models was performed using simple bright ‘blob’ detection implemented a custom Python script.

Pre-processing of plate-based scRNA-seq data

BAM files were converted to merged, de-multiplexed FASTQs using the Illumina provided Bcl2Fastq software package v2.17.1.14. Paired-end reads were mapped to the UCSC mm10 mouse transcriptome using Bowtie ([Langmead et al., 2009](#)) with parameters “-q-phred33-quals -n 1 -e 99999999 -l 25 -l 1 -X 2000 -a -m 15 -S -p 6,” which allows alignment of sequences with one mismatch. Expression levels of genes were quantified as transcript-per-million (TPM) values calculated by RSEM v1.2.3 in paired-end mode. For each cell, we quantified the number of genes for which at least one read was mapped, and then excluded all cells with either fewer than 3,000 detected genes or a transcriptome-mapping rate of less than 40%.

Selection of variable genes was performed by fitting a generalized linear model to the relationship between the squared coefficient of variation (CV) and the mean expression level in log/log space, and selecting genes that significantly deviated ($p < 0.05$) from the fitted curve, as previously described ([Brennecke et al., 2013](#)).

Pre-processing of droplet-based scRNA-seq data

De-multiplexing, alignment to the mm10 mouse transcriptome and UMI-collapsing were performed using the Cellranger toolkit (version 1.0.1) provided by 10X Genomics. For each cell, we quantified the number of genes for which at least one read was mapped, and then excluded all cells with fewer than 800 detected genes. In analyzing CD45⁺ immune cells, we excluded all cells with fewer than 250 detected genes. Expression values E_{ij} for gene i in cell j were calculated by dividing UMI count values for gene i by the sum of the UMI counts in cell j , to normalize for differences in coverage, and then multiplying by 10,000 to create TPM-like values, and finally calculating $\log_2(\text{TPM}+1)$ values. Batch correction was performed using ComBat ([Johnson et al., 2007](#)) as implemented in the R package sva using the default parametric adjustment mode. The output was a corrected expression matrix, which was used as input to further analysis. We identified highly variable genes as described above.

Dimensionality reduction by PCA

We restricted the expression matrix to the subsets of variable genes and high-quality cells noted above, and values were centered and scaled before input to PCA, which was implemented using the R function ‘prcomp’ from the ‘stats’ package for the plate-based dataset. For the droplet-based data, we used a randomized approximation to PCA, implemented using the ‘rpca’ function from the ‘rsvd’ R package, with the parameter k set to 100. This low-rank approximation is several orders of magnitude faster to compute for very wide matrices. After PCA, significant PCs were identified using a permutation test as previously described ([Buja and Eyuboglu, 1992](#)), implemented using the ‘permutationPA’ function from the ‘jackstraw’ R package. Only scores from these significant PCs were used as the input to further analysis.

tSNE visualization

For visualization purposes only (and *not* for clustering), dimensionality was further reduced using the Barnes-Hut approximate version of the *t*-distributed stochastic neighbor embedding (tSNE) ([van der Maaten, 2014](#)). This was implemented using the ‘Rtsne’ function from the ‘Rtsne’ R package using 20,000 iterations and a perplexity setting that ranged from 10 to 30 depending on the size of the dataset. Scores from the first n PCs were used as the input to tSNE, where n was determined for each dataset using the permutation test described above.

Removing doublets

In the plate-based dataset, several cells were outliers in terms of library complexity, which could possibly correspond to more than one individual cell per sequencing library, or ‘doublets’. As a precaution, we removed any cells in the top quantile 1% of the distribution of genes detected per cell, as these may correspond to doublets.

k-NN graph-based clustering

To cluster single cells by their expression profiles, we used unsupervised clustering, based on the Infomap graph-clustering algorithm (Rosvall and Bergstrom, 2008). Briefly, we constructed a k nearest neighbor (k -NN) graph on the data using as the metric for each pair of cells, the distance between the scores of significant PCs. The parameter k was chosen in a manner roughly consistent with the size of the dataset (Table S2). Specifically, k was set to 600, 200 and 50 for the droplet dataset of 23,177, 4,332 and 1,090 cells from combined T cell and cytokines, IL-13-treated and Th1 co-cultured organoids, respectively. For *in vivo* mouse models, k was set to 100, 300, 175, and 100 for nude mice, TCR β KO, Foxp3-DTR and MHCII $^{\Delta\text{gut}}$ respectively. For sub-clustering of stem cell subsets, we used $k = 150$ and $k = 40$ for the 637. The combined *Salmonella* and *H. polygyrus* infection dataset contained 5,122 immune cells and k was set to 200. The k -NN graph was computed using the function ‘nng’ from the R package ‘cccd’ and was then used as the input to Infomap (Rosvall and Bergstrom, 2008), implemented using the ‘infomap.community’ function from the ‘igraph’ R package. For k -NN graph-based clustering of the 24,649 CD45 $^{+}$ immune cells, the ‘FindClusters’ function from R package ‘Seurat’ was used with the resolution parameter set to 1.

Detected clusters were annotated by cell types or states using known markers for IEC subtypes (Sato et al., 2009). Specifically, for each known epithelial type we selected five canonical marker genes (e.g., *Lgr5*, *Ascl2*, *Slc12a2*, *Axin2* and *Olfm4* for stem cells, or *Lyz1*, *Defa17*, *Defa22*, *Defa24* and *Ang4* for Paneth cells), and scored all clusters for their expression (see below for signature scoring procedure). In all cases, one cluster unambiguously expressed each cell-type signature, with two exceptions: in the plate-based dataset, two clusters both expressed high levels of Lgr5 $^{+}$ ISC markers and accordingly were merged to form a ‘Stem’ cluster and two other clusters were merged to form a ‘TA’ cluster based on high expression of cell-cycle genes and low-to-moderate expression of Lgr5 $^{+}$ ISC genes. In the case of the CD45 $^{+}$ immune cells, the following markers were used to interpret clusters post hoc. B cells: *Bank1*, *Fcer2a*, *Cd79a*, *Cd79b*, *Cd22*. B cell (cycling): *Mki67*, *Cd79a*, *Cd79b*, *Ms4a1*, *Pou2af1*. Cd4 $^{+}$ T helper cells: *Cd4*, *Foxp3*, *Gata3*, *Cd3g*, *Tnfrsf4*. Cd8 T cells: *Gzma*, *Gzmb*, *Cd8a*. Dendritic cells (DCs): *Itgae*, *Tlr3*, *Cd209a*, *Cd209b*, *Irf8*, *H2-Ab1*, *Clec9a*. Epithelial: *Epcam*, *Krt8*, *Vil1*, *Muc2*, *Krt20*. Inflammatory monocytes: *Ccr2*, *Ly6c2*, *Fcgr1*, *Ifitm3*, *Fn1*. Neutrophils: *S100a9*, *S100a8*, *Csf3r*, *Cxcr2*, *Msrb1*, *Ccr1*. Natural Killer (NK) cells: *Ncr1*, *Prf1*, *Klra1*, *Xci1*. Plasmacytoid dendritic cells: *Siglech*, *Bst2*, *Tlr7*. Plasma cell: *Jchain*, *Mzb1*, *Xbp1*, *Sdc1*.

Assigning the three Lgr5 $^{+}$ ISC states to region of origin using supervised classification

To study the anatomical distribution of ISCs in different parts of the small intestine, we used a classification approach. First, we developed a classifier for the anatomical origin of Lgr5 $^{+}$ ISCs using single-cell expression profiles of 2,965 ISCs extracted from duodenum, jejunum, and ileum (Haber et al., 2017), by compiling a discriminative feature set using the expression levels of all genes differentially expressed (FDR < 0.1, Mann-Whitney U-test, log₂ fold-change > 0.25) between stem cells from the three regions, and also the scores along the first 25 PCs. A ‘random forest’ classifier was trained on these features, and subsequently distinguished between Lgr5 $^{+}$ ISCs from the three regions with an average out-of-bag accuracy of 92.9%. Finally, we used the trained classifier to classify the 637 ISCs (Figure 1) and infer the fraction of cells drawn from each intestinal region found in each ISC state (Figure S1F).

Cell-cell similarity matrix

To visualize heterogeneity of Lgr5 $^{+}$ ISCs within the ‘Stem’ cluster (637 cells), cell-cell similarities were computed. Principal component (PC) scores for each cell were computed across the 637 cells using the R function ‘prcomp’ as described above. The distance between cell i and j was calculated as the Pearson correlation between the scores of these two cells along the first 10 PCs. This distance matrix was then ordered using the k -NN graph-based cluster assignments described above, and visualized as a heatmap using the R function ‘aheatmap’.

Cell-cycle and Lgr5 $^{+}$ ISC subset signatures

To identify maximally specific genes associated with the three ISC subsets, we performed differential expression tests between each possible pairwise comparison between clusters. To ensure specificity of the detected marker genes to stem cells, the set of clusters included both the three ISC subsets (3 clusters), and all other detected IEC clusters (8 clusters) for a total of 11 clusters. Then, for a given cluster, putative signature genes were filtered using the maximum FDR Q-value and ranked by the minimum log₂(fold-change). The minimum fold-change and maximum Q-value represents the weakest effect-size across all pairwise comparisons, therefore this is a stringent criterion. Lgr5 $^{+}$ ISC subset signatures (Table S1) were obtained using a maximum FDR of 0.25 and a minimum log₂(fold-change) of 0.25. To exclude the explicit effect of known cell-cycle genes on the gene signature of the ISC subsets we filtered out any gene annotated as directly participating in cell-cycle regulation. Annotated cell-cycle genes were downloaded from the gene ontology (GO): <http://amigo.geneontology.org/amigo/term/GO:0007049>, and any gene appearing on this list was removed from the signature gene sets.

Gene sets associated with G1/S and G2/M phases of the cell-cycle were downloaded from <https://www.cell.com/cms/attachment/2051395126/2059328514/mmc2.xlsx> (Macosko et al., 2015). A set of cell-cycle genes to assess overall proliferation (see below for scoring procedure) was defined as the union of the G1/S and G2/M sets.

Scoring cells using signature gene sets

To score a specific set of n genes in a given cell, a ‘background’ gene set was defined to control for differences in sequencing coverage and library complexity between cells (Kowalczyk et al., 2015). The background gene set was selected to be similar to the genes of interest in terms of expression level. Specifically, the $10n$ nearest gene neighbors in the 2-D space defined by mean expression and detection frequency across all cells were selected. The signature score for that cell was then defined as the mean expression of the n signature genes in that cell, minus the mean expression of the $10n$ background genes in that cell.

Pseudo-time analysis of stem and progenitor cell differentiation

We used diffusion maps (Haghverdi et al., 2015) to order both *in vivo* stem and progenitor cells and the organoid IECs according to their differentiation state. For *in vivo* IECs, diffusion maps were computed for all cells together. In the case of organoids, for each of the two cytokines with the strongest effect on the stem cell pool (IL-10 and IL-13; Figure 2D), we build independent diffusion maps, along with their matched control organoids, using the function ‘DiffusionMap’ from the R package ‘destiny’, using only a set of highly variable genes that were selected as described above.

Since the major source of variability among these cells was differentiation, we reasoned that diffusion pseudotime would likely reflect the progression along an axis from stem to mature IECs. Specifically, the diffusione pseudotime is a relative metric and measures the distance between each cell and a specified root cell. We use the intestinal stem cell as the root since it is a natural starting point from which to measure developmental progression. As there is only a single pseudotime axis, this represents development progress across multiple trajectories and reflects the stem-differentiation axis in general (rather than branching to specific lineages). Indeed, for organoids, there was a high correlation between pseudotime n (calculated using the function ‘DPT’), and a stemness signature score, computed using 10 known Lgr5 $^{+}$ ISC markers (as in Figures S1A and S1I) (Spearman $|p| = 0.70$ for IL-10 and $|p| = 0.66$ for IL-13, $p < 2 \times 10^{-16}$ in both cases). We performed a further optimization step by varying the diffusion map’s Gaussian kernel width parameter (σ), and selecting the value that maximized p in each case. The resulting values were $\sigma = 8$ for both IL-10 and IL-13.

For *in vivo* IECs, diffusion component 1 (DC-1) was strongly correlated with the expression of the stemness signature score ($r = 0.83$, Figure S1I), and the score of each cell along DC-1 was therefore selected as the pseudotime axis. In all cases, the significance of differences in the distribution of cells along the pseudo-time axis were computed using the Mann-Whitney U-test.

Testing for shifts in cell proportions in intestinal organoids

Under several conditions, we observed dramatic changes in the frequency of epithelial cell subtypes. The statistical significance of these shifts was assessed by calculating, for each condition comparison and cell type, the exact hypergeometric probability (without replacement) of the observed change in cell numbers.

Specifically, given that m and n total cells (of all cell types) are sequenced in a treatment and control condition respectively, we test, for a given cell type, whether the number of k and q of observed cells of type **C** in total and treatment condition respectively, significantly deviates from a null model given by the hypergeometric distribution. The probability of observing these values was calculated using the R function ‘phyper’ from the ‘stats’ package, using the command:

```
p = phyper(q, k, m, n)
```

and was reported as a hypergeometric p value. Confidence intervals for the odds-ratio were computed using the R function ‘fisher.test’.

Testing for shifts in cell proportions *in vivo*

In the case of *in vivo* perturbation experiments, we used a regression model to control for any mouse-to-mouse variability among our biological replicates. For each cell-type, we model the number of cells detected in each analyzed mouse as a random count variable using a negative binomial distribution. The rate of detection (as a fraction of all cells) is then modeled by using the natural log of the total number of cells profiled in a given mouse as an offset variable. The genotype of each mouse (i.e., knockout or WT) was provided as a covariate. The model was fit using the R command ‘glm.nb’ from the ‘MASS’ package. The p value for the significance of the effect produced by the knockout was then assessed using a likelihood-ratio test computed using the R function ‘anova’.

GO analysis

GO analysis was performed using the ‘goseq’ R package (Young et al., 2010), using significantly differentially expressed genes ($FDR < 0.05$) as target genes, and all genes expressed with $\log_2(\text{TPM}+1) > 3$ in at least 10 cells as background.

Analysis of CD4 $^{+}$ T helper cell activation in MHCII $^{\text{gut}-/-}$ mice

Differential expression analysis of 1,150 CD4 $^{+}$ T helper cells (Table S5) under homeostasis was conducted using the ‘MAST’ R package, and the upregulated genes ($FDR < 0.01$, likelihood-ratio test and \log_2 fold-change > 0.1) were tested for enrichment among the 495 genes in the ‘T cell activation’ GO term (GO:0042110) by the hypergeometric test using the R function ‘fisher.test’. We note that due to the lower numbers of CD4 $^{+}$ T helper cells in the *H. polygyrus* condition, the same DE test revealed no differentially expressed genes between the MHCII $^{\text{gut}-/-}$ and matched controls.

As a confirmatory analysis, we also scored (using the procedure described above) the CD4⁺ Th cells from all conditions for set of 13 canonical T cell activation markers: *Cd28*, *Cd40lg*, *Cd44*, *Cd69*, *Ctla4*, *Dpp4* (CD26), *Havcr2* (TIM-3), *Icos*, *Il2ra* (CD25), *Lag3*, *Pdcdf* (PD1), *Tfrc* (CD71) and *Tigit*, and tested for differences in the signature score between conditions using the Mann-Whitney U-test.

DATA AND SOFTWARE AVAILABILITY

The accession number for all raw and processed single-cell RNA sequencing data reported in this paper is GEO: GSE106510.

Python code for mRNA quantification from smFISH images can be found in the following repository: https://github.com/adamh-broad/image_analysis.

Raw data can be found in Mendeley: <https://data.mendeley.com/datasets/9rvb5p2ydh/edit>

Additional Resources

Single Cell Portal (https://portals.broadinstitute.org/single_cell/intestinal_stem_cell)

Supplemental Figures

Cell

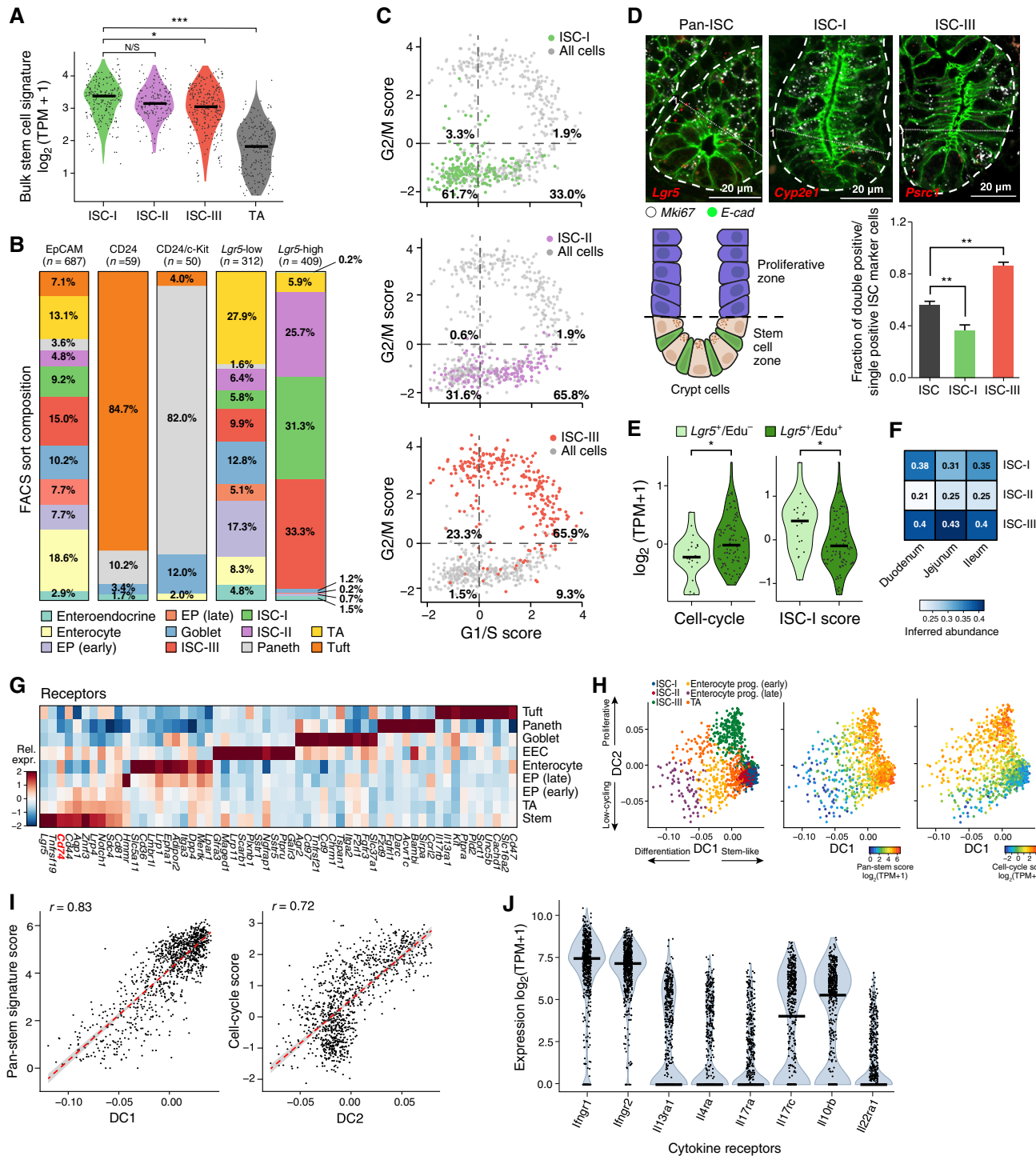


Figure S1. Identification of *Lgr5*⁺ Stem Cells by scRNA-Seq, Related to Figure 1

- (A) All *Lgr5*⁺ ISC subsets express known ISC signature. Violin plot of the distribution of mean expression ($\log_2(\text{TPM} + 1)$, y axis) of stem cell signature genes (Muñoz et al., 2012), in each of the three ISC subsets and in 201 TA progenitors (x axis). * $p < 0.001$, ** $p < 1 \times 10^{-5}$, *** $p < 1 \times 10^{-7}$ (Mann-Whitney U-test).
- (B) All three ISC subsets comprise *Lgr5*⁺ ISCs based on FACS in *Lgr5*-GFP mouse model (Barker et al., 2007). Proportion (percentage, y axis) of cells from each identified cluster (color legend) in each of the FACS fractions (bars). 90.3% of cells in the *Lgr5*^{high} fraction are assigned to one of the three *Lgr5*⁺ ISC subsets; the three ISC subsets were strongly enriched for GFP^{high} cells (*Lgr5*^{high}). EP: Enterocyte progenitor, EEC: enteroendocrine cells.
- (C) Distinct cell-cycle characteristics of each of the three *Lgr5*⁺ ISC subsets. Scatterplots of the signature score for 637 *Lgr5*⁺ ISCs (points, STAR Methods) for G1/S genes (x axis) and G2/M genes (y axis) (signatures from (Kowalczyk et al., 2015; Tirosh et al., 2016)). Cells are colored by their cluster assignment to subsets.

(legend continued on next page)

- (D) Validation of ISC subsets and their cell cycle status. Upper panels: Combined smFISH and IFA of FFPE sections of intestinal tissue from WT mice for the pan-stem cell marker *Lgr5* (upper left), ISC-I marker *Cyp2e1* (upper middle) and ISC-III marker *Psrc1* (upper right) all in red and *Mki67* in white. Cell borders were assessed with E-cadherin (green); scale bar, 20 μ m. Bottom left: Schematic of the lower crypt fraction ('stem cell zone'), in which co-expression of stem cell markers (*Lgr5*, *Cyp2e1* or *Psrc1*) and the proliferation marker *Mki67* was quantified. Bottom right: Bar plot of the fraction (y axis) of cells which are positive for *Mki67* out of all cells positive for each stem cell marker. n = 4 mice, 10 crypts on average per mouse (**p < 0.0025, t test; error bars: SEM).
- (E) Enrichment of ISC-I in EdU⁻ cells confirms they are in a low-cycling state. Violin plots of the distribution of signature scores for the cell cycle (left) and ISC-I subset (right, signature as in Table S1) from FACS sorted EdU⁻ *Lgr5*⁺ ISCs (light green) or EdU⁺ *Lgr5*⁺ ISCs (dark green) after *in vivo* EdU labeling and single nucleus RNA-seq using Div-Seq (Habib et al., 2016). *p < 0.05, Mann-Whitney U-test.
- (F) Three ISC subsets are similarly represented along the small intestine. Fraction (color legend) of cells in each of the ISC subsets (rows) among the ISCs isolated from each of three spatial regions (columns), as inferred using a random forest classifier trained on 2,965 ISCs (Haber et al., 2017).
- (G) Cell type-enriched receptors. Average relative expression (Z-score of mean log₂(TPM+1), color bar) of the top 10 receptors (columns) enriched (FDR < 0.05, Mann-Whitney U-test) in each cell type (rows). The invariant chain of MHCII, *Cd74*, is highlighted in red. H,I. Pseudotime analysis of IECs.
- (H) Diffusion maps of intestinal epithelial stem and progenitor cells. Scatterplot of the scores along the first two diffusion components (DCs, STAR Methods) for each of 1,022 stem and progenitor epithelial cells (points) colored by cluster label (left), bulk stem cell signature score (middle) and cell-cycle signature score (right).
- (I) Diffusion components (DCs) associated with differentiation (DC1) and the cell cycle (DC2). Scatterplots showing for each cell its (left) DC-1 score (x axis) versus bulk stem cell score (y axis) and (right) DC-2 score versus cell-cycle score (y axis, right). Pearson's correlation and linear regression fit (dashed red line) are shown.
- (J) Cytokine receptors expressed by ISC. Violin plots of the distribution of expression levels (log₂(TPM+1), y axis; bar: median) of different cytokine receptors (x axis) in ISCs.

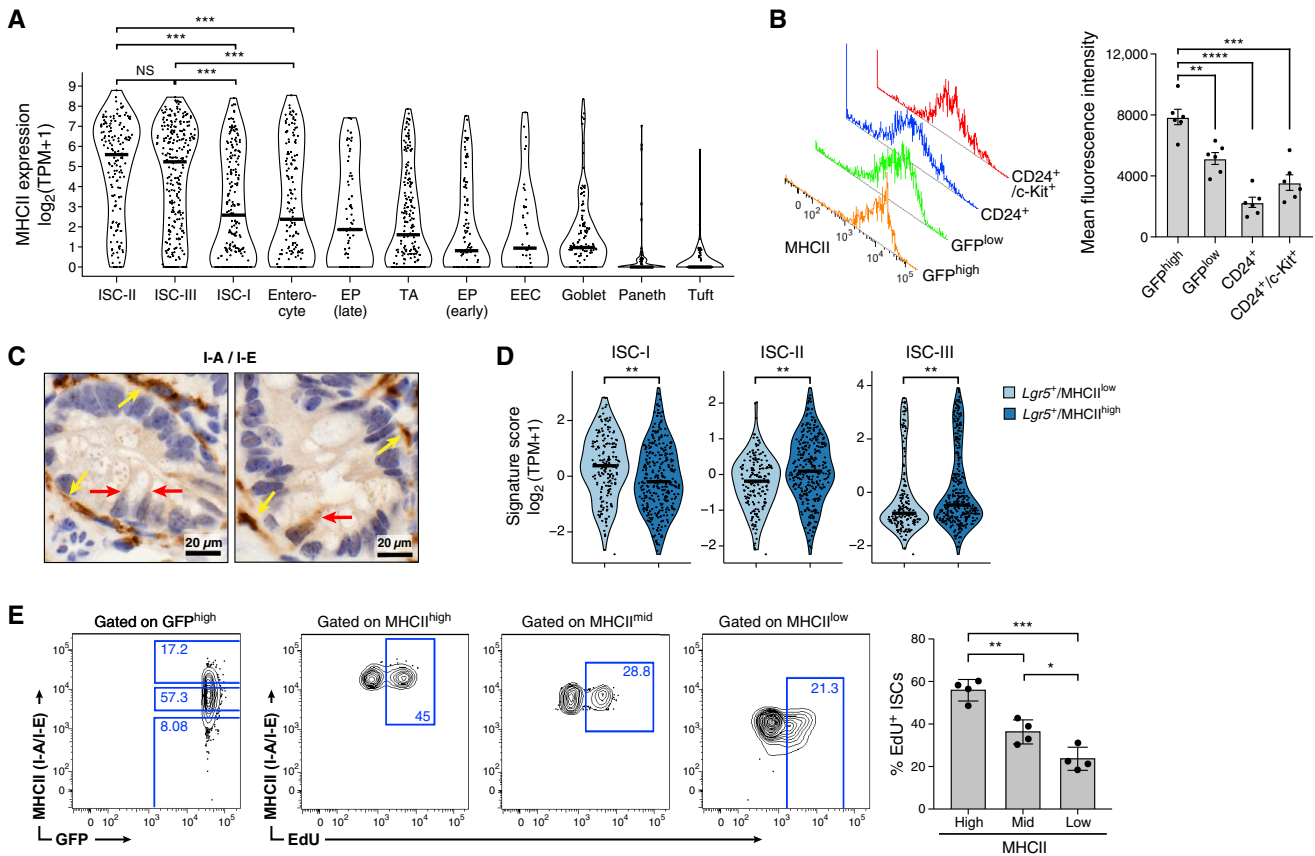


Figure S2. Identification and Characterization of MHCII-Expressing Lgr5⁺ ISCs, Related to Figure 1

(A) MHCII signature is largely restricted to ISCs. Violin plot of the distribution of mean expression levels ($\log_2(\text{TPM}+1)$, y axis, bar: median) of MHCII genes (*H2-Ab1*, *H2-Aa*, *Cita*, *Cd74*, *H2-DMA*, *H2-DMb1*) in each IEC type from 1,522 IECs profiled by full-length scRNA-seq. EP: Enterocyte progenitor, EEC: enteroendocrine cell. *** $p < 0.001$, Mann-Whitney U-test.

(B) MHCII protein expression in IECs from Lgr5-GFP mouse. Distribution (left) and mean (bar plot, right) of detected fluorescence by FACS corresponding to MHCII protein expression in populations sorted for GFP^{high} (Lgr5⁺ ISC), GFP^{low} (TA), CD24⁺ (tuft and enteroendocrine) or CD24⁺/c-Kit⁺ (Paneth and goblet). * $p < 0.01$, ** $p < 0.001$, *** $p < 0.0001$, t-test; error bars: SEM, $n = 6$ mice.

(C) MHCII is expressed in intestinal crypts of WT mice. IHC images show MHCII expression (I-A/I-E, brown) within crypts of WT mice ($n = 2$ mice). Red arrows, MHCII⁺ IEC. Yellow arrows, Lamina propria (LP) MHCII⁺ cells. Scale bar, 20 μm.

(D) MHCII^{high} Lgr5⁺ ISCs are enriched for ISC-II and ISC-III subsets and depleted of ISC-I subset. Violin plots of the distribution of signature scores (as in Table S1) for ISC-I, -II, and -III subsets, in scRNA-seq profiles from 326 Lgr5⁺MHCII^{high} (light blue) and 177 Lgr5⁺MHCII^{low} (dark blue) cells (individual black dots). Horizontal black line denotes the median (* $p < 0.001$, Mann-Whitney U-test).

(E) Higher proliferation of Lgr5⁺ ISCs with high MHCII expression. Left: FACS plots of Lgr5⁺ ISCs gated on GFP^{high} (Lgr5⁺, left) binned into subsets of low, intermediate and high MHCII expression (middle panels, y axis), and then gated on EdU incorporation (middle panels, x axis). Right: Bar plot of the fraction (percentage, y axis) of EdU⁺ cells within each MHCII expression level ($n = 4$ mice, * $p < 0.05$, ** $p < 0.005$, *** $p < 0.0005$, t test, error bars: SEM).

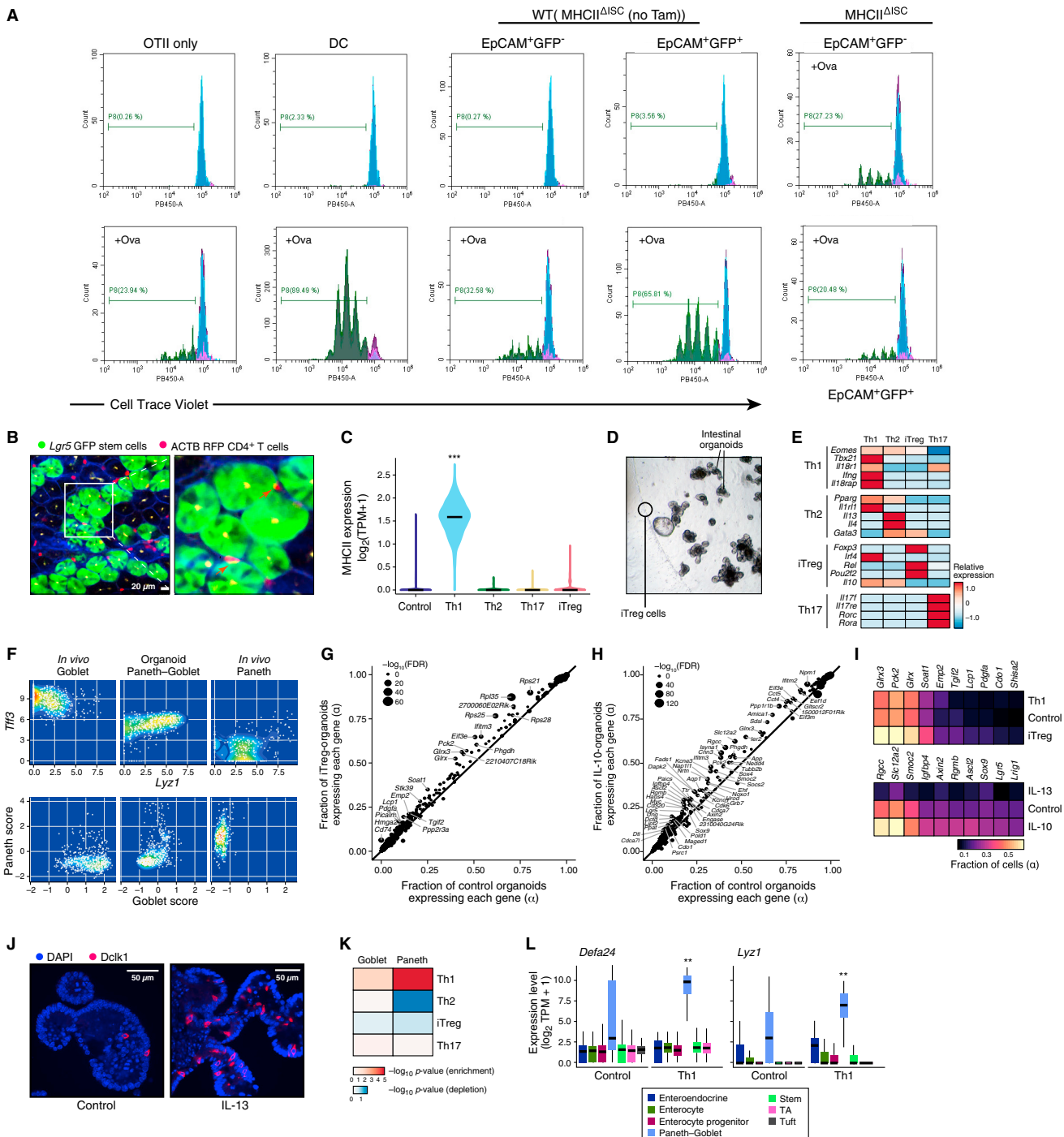


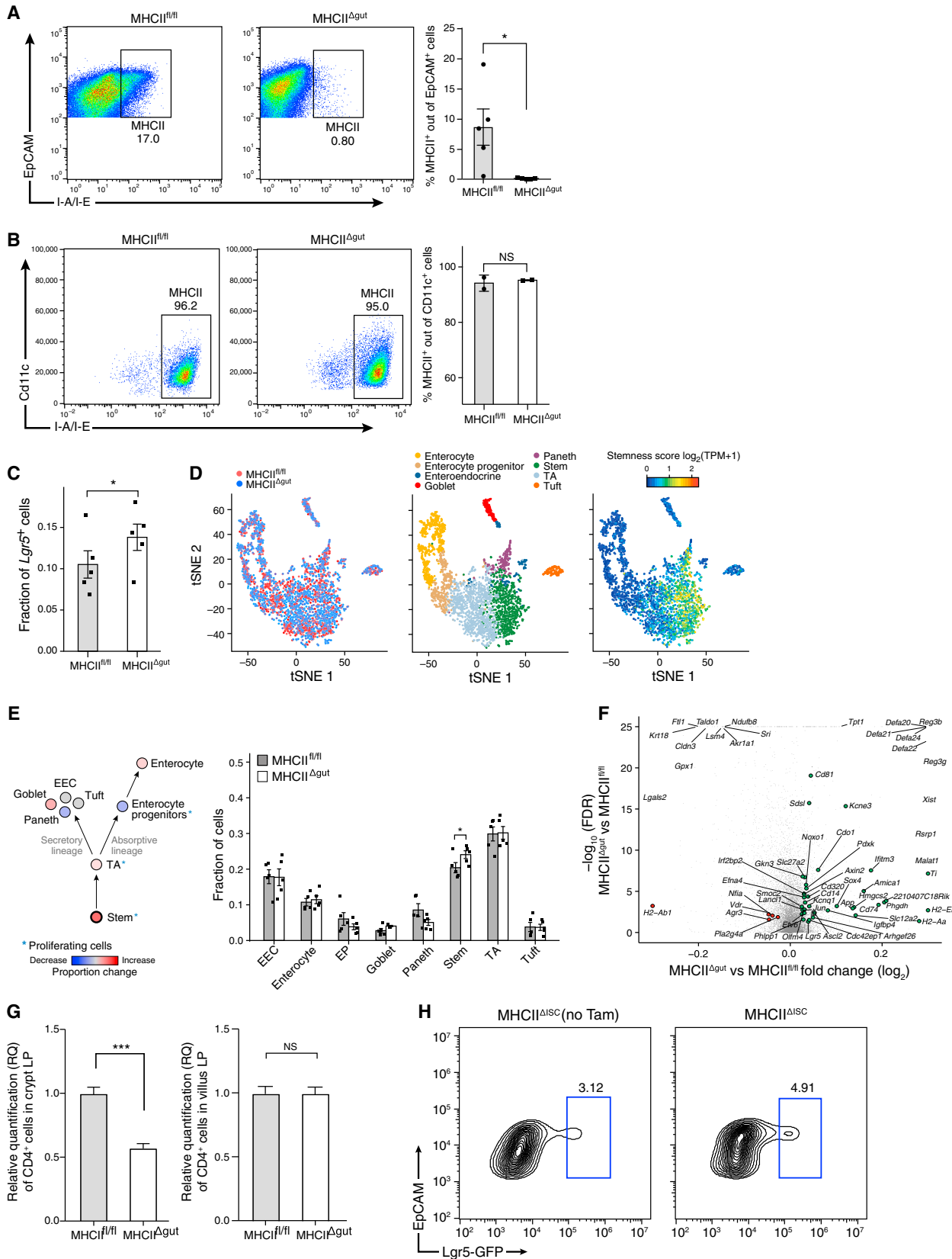
Figure S3. Antigen Presentation by ISCs and the Impact of Th Cytokines on IEC Differentiation, Related to Figure 2

(A) Lgr5⁺ ISCs induce CD4⁺ Th cell proliferation *in vitro*. Representative FACS histograms of cell trace violet-labeled naive CD4⁺ T cells from OTII mice that were cultured alone or with DC, EpCAM^{+GFP}⁺ and Lgr5-GFP⁺ ISCs (EpCAM^{+GFP}⁺) from WT (MHCII^{ΔISC} (no Tam)) mice, which express H2-Ab1 or EpCAM^{+GFP}⁺ (Top right) and Lgr5-GFP⁺ ISCs (EpCAM^{+GFP}⁺, bottom right) from MHCII^{ΔISC} mice (no expression of H2-Ab1). Cells treated with OVA peptide (15 µg/mL) are labeled with +Ova in the plot. Percentage of proliferating cells is indicated by the gate in each plot.

(B) CD4⁺ T cells interact with Lgr5⁺ISCs *in vivo*. Two-photon microscopy image of the small intestine from the mosaic *Lgr5-GFP* (green) knock-in mouse engrafted with RFP⁺ CD4⁺ T cells (red). See related [Video S1](#). CD4⁺ T cells are visible in close proximity to Lgr5⁺ ISCs (red arrows in inset showing yellow as red and green overlap, right). Scale bar, 20 μ m. Yellow spots in the middle of the green and blue crypts indicate non-specific fluorescence. Blue crypts reflect Lgr5-GFP⁺ ISCs, typical of this mosaic mouse.

(legend continued on next page)

- (C) Induction of MHCII expression in organoids co-cultured with Th1 cells. Violin plot of the distribution of mean expression levels ($\log_2(\text{TPM}+1)$, y axis, bar: median) of six MHCII genes (*H2-Ab1*, *H2-Aa*, *Ciita*, *Cd74*, *H2-DMa*, *H2-DMb1*) in IECs profiled by scRNA-seq of 6,234 cells from control organoids and those co-cultured with each subset of Th cells (x axis). *** $p < 10^{-10}$, Mann-Whitney U-test.
- (D) Intestinal organoids co-cultured with iT_{reg} cells. Image at $\times 4$ magnification. Lines: T_{reg}s or organoids.
- (E) Validation of *in vitro*-polarized Th cell populations. Mean relative expression (row-wise Z-score of mean $\log_2(\text{TPM}+1)$ values, color bar) of canonical marker genes (rows) in the cells from each *in vitro*-differentiated Th cell subset (columns), from scRNA-seq of the co-cultures.
- (F) Organoid-derived secretory IECs co-express markers for goblet and Paneth cells. Scatterplots of the expression levels (top row, $\log_2(\text{TPM}+1)$) of canonical markers for goblet cells (*Tff3*, y-axis) and Paneth cells (*Lyz1*, x-axis) or signature scores for goblet and Paneth cells (bottom row, 50 genes), for *in vivo* goblet cells (left), cells in the Paneth-goblet cluster from control organoids (middle) and *in vivo* Paneth cells (right).
- (G-I) Changes in proportion of cells expressing stem cell marker genes after co-culture with induced T_{reg} cells (iT_{reg}s) or treatment with IL-10. G,H. Scatterplots compare the fraction of cells with non-zero expression (α , y axis) of each gene (dot) in organoids co-cultured with iT_{reg}-cells (G) or treated with IL-10 (H), compared to the fraction in matching control organoids (α , x axis). All upregulated genes are shown (FDR < 0.05), sized relative to significance (- $\log_{10}(\text{FDR})$, legend top left). Several key Lgr5⁺ ISC marker genes are labeled. Diagonal line: no change relative to control organoids. (I) Heatmap of the fraction of cells with non-zero expression (α , color bar) of 10 selected stem cell marker genes (columns) within organoids co-cultured with iT_{reg}s or Th1 cells (top, rows) or treated with IL-13 or IL-10 cytokines (bottom, rows). All genes are expressed at a larger proportion of cells (FDR < 0.05, Mann-Whitney U-test) in organoids co-cultured with iT_{reg} cells (top) or treated with IL-10 (bottom), compared to control organoids.
- (J) Dclk1⁺ tuft cell expansion following IL-13 treatment. IFA of Dclk1 (red) in control organoids (left) and IL-13-treated organoids (right). DAPI: blue, scale bar, 50 μm .
- (K and L) Upregulation of Paneth cell-related gene expression in Th1 co-cultured organoids. (K) Significance of change in Paneth and goblet cell signature scores (columns) in 'Paneth-goblet' cells between different Th co-cultures (rows) and control organoids (- $\log_{10}(p\text{-value})$, Mann-Whitney U-test, color bar, of enrichment (red) and depletion (blue)). (L) Boxplots of the distribution of expression levels ($\log_2(\text{TPM}+1)$, y axis) of canonical Paneth cell markers *Defa24* (left) and *Lyz1* (right) in the IEC-type cluster (x axis) from organoids co-cultured with Th1 cells (right part of each panel) compared to control organoids (left part). ** $p < 10^{-5}$ (Mann-Whitney U-test). Black bar, median value; box edges, 25th and 75th percentiles; whiskers, a further 1.5 times the interquartile range.



(legend on next page)

Figure S4. An Expanded Lgr5⁺ ISC Pool in MHCII^{Δgut} or MHCII^{ΔISC} Mice, Related to Figure 3

(A and B) Epithelial cell specific MHCII knockout (MHCII^{Δgut}) mice. FACS quantification of MHCII-expressing IECs in small intestine (A) and mesenteric lymph node (B). Scatterplots (left) and bar plots (right) show the percentage of EpCAM⁺ MHCII⁺ (A) or CD11c⁺ MHCII⁺ (B) cells in MHCII^{f/f} and MHCII^{Δgut} mice. (A) n = 5 mice, *p < 0.05. (B) n = 2 mice, NS: not statistically significant, t test, error bars: SEM.

(C) Increased proportion of *Lgr5* expressing cells in MHCII^{Δgut} mice. Fraction of cells (y axis) in which the transcript for *Lgr5* is detected, among the 1,559 cells profiled from MHCII^{Δgut} mice (n = 5) and 1,617 cells profiled from matched MHCII^{f/f} controls (n = 5). Error bars: SEM, *p < 0.05, likelihood-ratio test.

(D) Cell subset identification in scRNA-seq of IECs from MHCII^{Δgut} and matched controls. tSNE of 3,176 cells colored by either genotype (left), cell type assignment by unsupervised clustering (middle), or stemness score (right; score as in Figure S1A).

(E and F) ISC expansion in MHCII^{Δgut}. (E) Right: The fraction of cells (y-axis) in each cell type from MHCII^{Δgut} (white bar) and matched MHCII^{f/f} controls (gray bar). EP: Enterocyte progenitor, EEC: enterendocrine cells. Left: schematic summary of changes in cell proportions along differentiation. Nodes: cell types; red: increase-, blue: decrease- in cell proportion; scale bar, bottom. Bold outline: statistically significant change; *proliferating cell type. Error bars: SEM. (*FDR < 0.05, likelihood-ratio test). (F) DE genes based on 1,559 cells in MHCII^{Δgut} mice (n = 5) versus 1,617 cells from matched MHCII^{f/f} controls (n = 5). Green dots: upregulated ISC genes, red dots: downregulated ISC genes (FDR < 0.05, likelihood-ratio test), gray dots: all other genes.

(G) Decreased proportion of CD4⁺ cells in the crypt lamina propria of MHCII^{Δgut} mice. Relative quantification (RQ) of CD4⁺ cells (y axis) per crypt lamina propria (LP) (left) or villus LP (right) in MHCII^{f/f} and MHCII^{Δgut} (x axis) relative to MHCII^{f/f} mice in homeostasis. n = 3 mice and 8 fields per mouse (**p < 0.0001, NS: not significant, t test, error bars: SEM).

(H) Elevated proportion of Lgr5⁺ ISCs in MHCII^{ΔISC} compared to control mice (MHCII^{ΔISC} (no Tam)). Representative FACS plot of IECs gated on GFP-high (Lgr5⁺ ISCs) (representative of n = 8 mice).

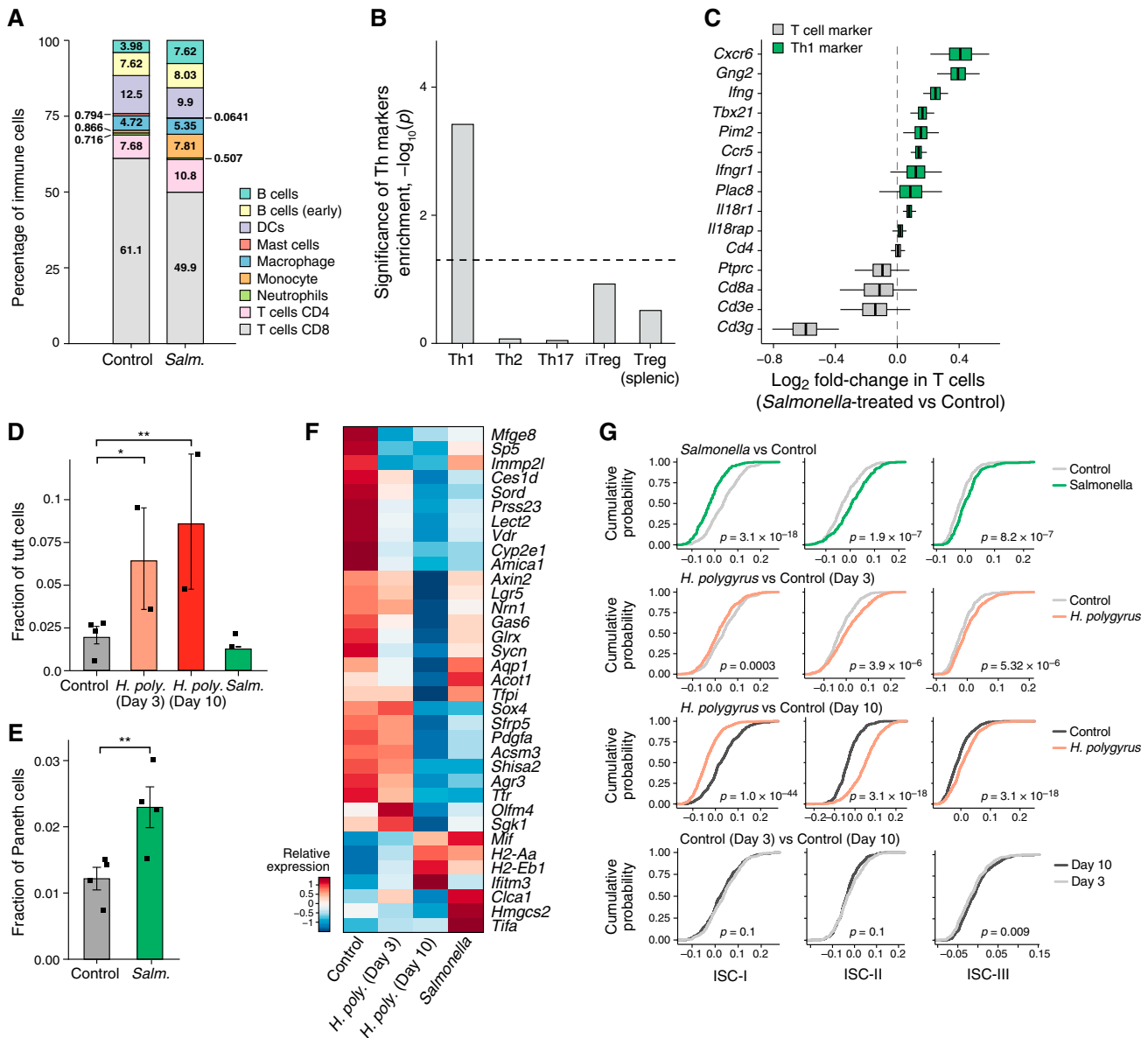


Figure S5. Changes in IEC Remodeling and ISC States upon Pathogenic Infections with or without MHCII Blockage, Related to Figure 4

(A–C) *S. enterica* infection induces Th1 polarization in the gut. (A) Percentage (y axis) of different immune cell subsets (color legend), as determined by scRNA-seq of 5,122 CD45⁺ cells from the lamina propria of control and *Salmonella*-infected mice (n = 5 control mice and n = 4 *Salmonella* infected mice). (B) Significance of enrichment ($-\log_{10}(p\text{-value})$, y axis, hypergeometric test) of marker genes for different Th subsets (x axis) among the genes induced (FDR < 0.05, likelihood-ratio test) in T cells from *Salmonella* infected versus control mice. Dashed line: p = 0.05 (n = 5 control mice and n = 4 *Salmonella* infected mice). (C) Differential expression (x axis) of each gene (y axis) across 824 T cells from *Salmonella*-infected mice (n = 4) and 543 T cells from control mice (n = 5). Bar indicates Bayesian bootstrap (Rubin, 1981) estimates of $\log_2(\text{fold-change})$; hinges and whiskers indicate 25% and 95% confidence intervals, respectively. Green: Th1 cell markers. Dashed line: no differential expression.

(D and E) Changes in fractions of tuft (D) and Paneth cells (E) within the intestinal epithelium after infection. Frequencies of tuft (D) and Paneth (E) cells (y axis), as determined by unsupervised clustering of scRNA-seq data in mice under different conditions (x axis) (Haber et al., 2017). n = 2 mice per helminth infected group and 4 mice per control and *Salmonella*-infected groups (points: individual mouse). * FDR < 10^{-5} ; ** FDR < 10^{-10} , likelihood-ratio test; error bars: SEM.

(F) Pathogenic infection reduces the expression of ISC marker genes. Mean expression (column-wise Z-score of mean $\log_2(\text{TPM}+1)$ values, color bar) of each known Lgr5⁺ ISC marker gene (Muñoz et al., 2012) (rows) that is differentially expressed (FDR < 0.01) by 1,857 ISCs from scRNA-seq, between control and pathogen-infected mice (columns).

(G) Changes in ISC subset proportions under infection *in vivo*. Cumulative distribution functions (y axis) of ISC-I, ISC-II and ISC-III signature scores (columns) (x axis, signatures as in Table S1) in 1,857 Lgr5⁺ ISCs from the infected mice (colored) versus controls (gray) (top three rows) or the controls at 3 and 10 days (bottom row). Mann-Whitney U-test p values are shown for the significance of changes in signature scores between the compared sets of ISCs.

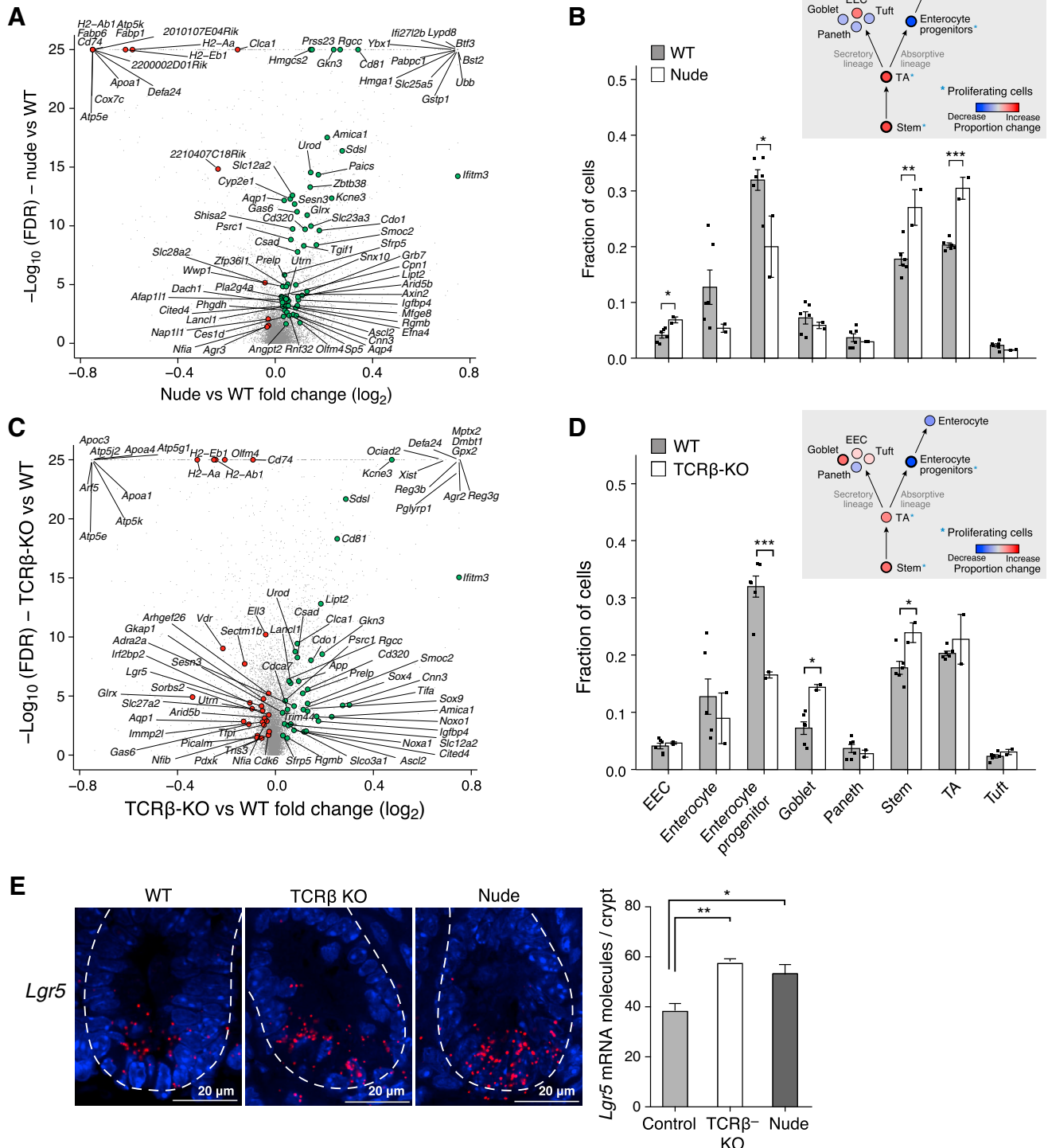


Figure S6. An Expanded Lgr5⁺ ISC Pool in T Cell-Depleted Mouse Models, Related to Figure 6

(A–D) ISC expansion in nude and TCRβ-KO mice by scRNA-seq. Differentially expressed genes (A,C) and changes in IEC frequencies (B,D) from 2,967 cells from nude mice (A,B, n = 2 mice) or 9,488 cells from TCRβ-KO mice (C,D) n = 2 mice versus 7,216 cells from WT mice controls (n = 6). (A,C) Mean log₂ fold-change (x axis) and significance (-log₁₀(FDR)) of differential expression. Green dots: upregulated ISC genes, red dots: downregulated ISC genes (FDR < 0.05, likelihood-ratio test), gray dots: all other genes. (B,D) Bar plots of fraction (y axis) of each major IEC-type (x axis) from unsupervised clustering, in cells from WT (gray) versus nude (white, B) or TCRβ-KO mice (white, D). Dots: individual mice. Error bars: SEM (* FDR < 0.05, ** FDR < 0.005, *** FDR < 10⁻⁵, likelihood-ratio test). Grey

(legend continued on next page)

inset: schematic summary of changes in cell proportions along differentiation. Nodes: cell types; red: increase-, blue: decrease- in cell proportion; scale bar, bottom right. Bold outline: statistically significant change; * proliferating cell type.

(E) Elevated *Lgr5* expression in nude and TCR β KO mice tested by smFISH of *Lgr5* in the crypt. Left: representative images of *Lgr5* (red) in crypts of WT (left), TCR β -KO (center), and nude (right) mice. Scale bar, 20 μ m. Right: Number of *Lgr5* molecules detected per crypt (y axis) in each of the three models (x axis). n = 2 mice and 8 fields per group. Error bars: SEM (*p < 0.05, **p < 0.005, t test).

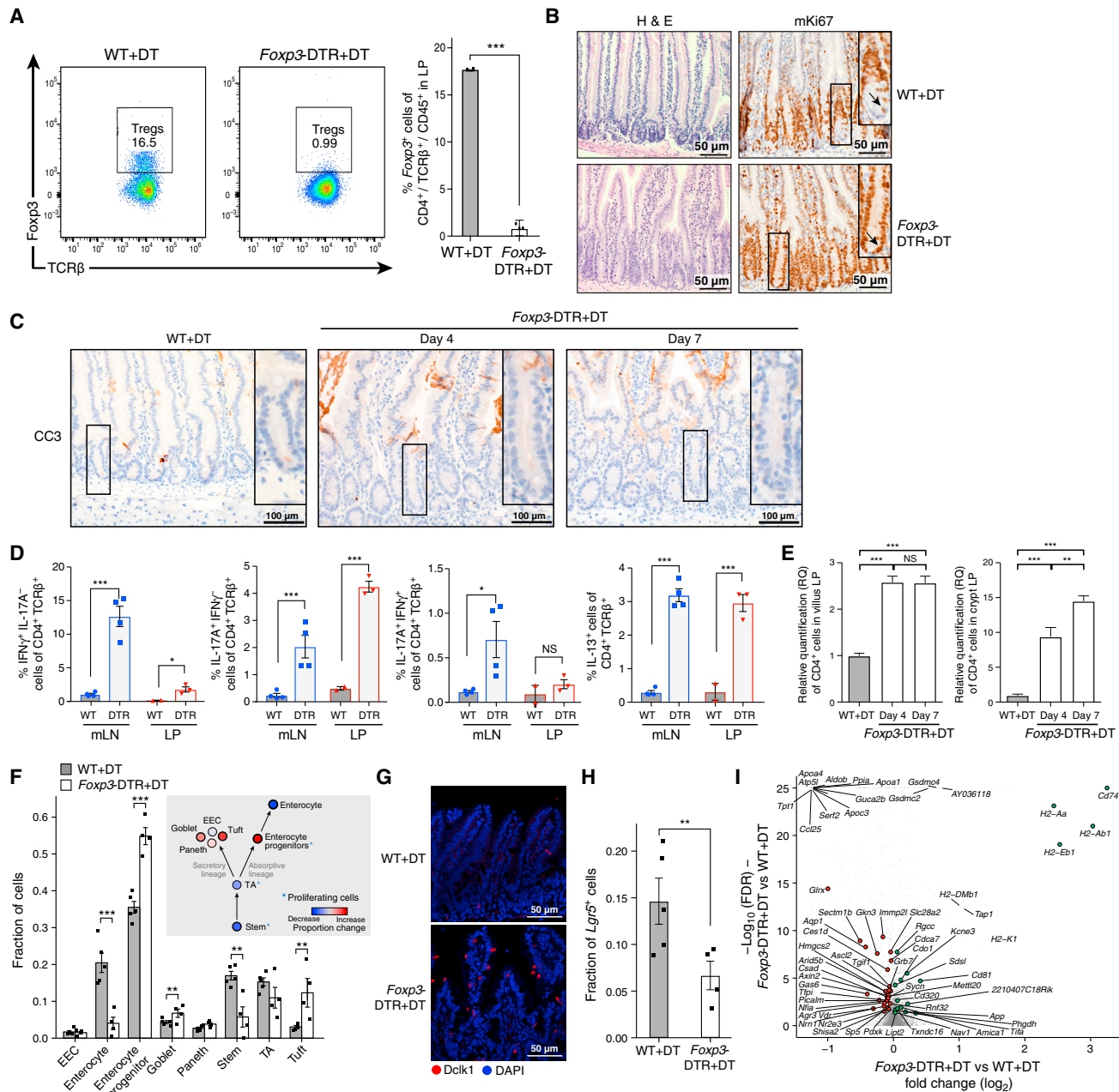


Figure S7. T_{reg} Depletion Reduces the Lgr5⁺ ISC Pool In Vivo, Related to Figure 6

(A) Validation of T_{reg} depletion. Representative FACS plot (left) and quantified mean proportion (bar plot, right) of TCR⁺ Foxp3⁺ cells out of all CD4⁺ TCR⁺ cells in the lamina propria (LP) of WT and Foxp3-DTR mice (y axis) after 7 days of DT treatment. Dots: individual mice. Error bars: SEM ($n = 3$ mice, *** $p < 0.0005$ t test).

(B) Increased proliferation at the bottom of intestinal crypts following T_{reg} depletion. FFPE sections stained for H&E (left) and mKi67 IHC (brown, right) in WT (top row) and Foxp3-DTR mice (bottom row) after 7 days of DT treatment. Inset is 3 \times magnification; arrow: mKi67⁺ cell. Scale bar, 50 μ m.

(C) No signs of apoptosis in the small intestine, particularly in Lgr5⁺ ISCs following T_{reg} depletion. IHC images of FFPE sections stained for cleaved-caspase 3 (CC3) after 4 or 7 days of DT induction. Inset is 3 \times magnification. D,E. Increase in other Th cells in the mesenteric lymph nodes and lamina propria following T_{reg} depletion.

(D) FACS quantification of the mean proportions (y axis) of IFN γ ⁺ (left), IL-17A⁺ (mid-left), IFN γ + IL-17A⁺ (mid-right) and IL-13⁺ (right) cells out of all CD4⁺ TCR⁺ cells in the mesenteric lymph nodes (mLN, $n = 4$ per group) or lamina propria (LP, $n = 3$ per Foxp3-DTR group and $n = 2$ per matched WT group) of the small intestine of WT and Foxp3-DTR mice (y axis) after 7 days of DT induction. * $p < 0.045$, *** $p < 0.0007$, t test, error bars: SEM.

(E) IFA relative quantification (RQ, y axis) of CD4⁺ cells per villus lamina propria (LP) (left) or crypt LP (right) in WT and Foxp3-DTR treated with DT for 4 and 7 days (x axis). $n = 2$ mice and 8 fields per mouse (** $p < 0.0001$, NS: not significant, t test, error bars: SEM).

(legend continued on next page)

